geosciences

MDPI

Article

Depositional Environments and Soft Sediment Deformation in the Early Jurassic Ammonitico Rosso Formation of Western Greece

Vasilis Golfinopoulos [1], David J. W. Piper [2], Avraam Zelilidis [1], Georgia Pe-Piper [3], Penelope Papadopoulou [1], Nicolina Bourli [1] and George Iliopoulos [1,*]

[1] Department of Geology, University of Patras, 265 04 Patras, Greece; gkolfinopoulosv@ac.upatras.gr (V.G.); a.zelilidis@upatras.gr (A.Z.); penelpapadop@upatras.gr (P.P.), n_bourli@ac.upatras.gr (N.B.)
[2] Department of Oceanography, Dalhousie University, Halifax, NS B3H 4R2, Canada; david.piper@canada.ca
[3] Department of Geology, Saint Mary's University, Halifax, NS B3H 3C3, Canada; gpiper@smu.ca
* Correspondence: iliopoulosg@upatras.gr

Abstract: This study investigates the depositional environments and soft sediment deformation within the Early Jurassic Ammonitico Rosso Formation in the External Ionian Basin (Western Greece), focusing on its biostratigraphy, sedimentology, and tectonic activity. This research provides new insights into the depositional environment of the Ammonitico Rosso Formation and its transitions with the underlying and overlying formations. Syn-rift tectonics at the time of deposition formed half-grabens, which influenced sedimentary processes and created conditions for seabed slumping. Detailed field mapping and microfacies analysis revealed two distinct depositional environments: deep-water to open-shelf settings and platform-margin reefs. The entire Ammonitico Rosso Formation is allochthonous, deposited as repetitive slices of little-disturbed stratified sediments capped by debrites near the toe of a complex submarine landslide. The presence of well-preserved fossils, such as planktonic and benthic foraminifera, Radiolaria (both Spumellaria and Nassellaria), and ammonites, allowed precise age determinations, suggesting that the first appearance of *Globuligerina* might predate previous records, occurring first in the Pliensbachian rather than the Toarcian. These findings contribute to the ongoing debate on the depth and conditions of Ammonitico Rosso deposition, supporting the hypothesis of a relatively deep, open-shelf environment influenced by slope instability.

Keywords: Ammonitico Rosso; slumps; Toarcian; planktonic foraminifera

Academic Editor: José Manuel Castro

Received: 30 October 2024
Revised: 24 December 2024
Accepted: 31 December 2024
Published: 4 January 2025

Citation: Golfinopoulos, V.; Piper, D.J.W.; Zelilidis, A.; Pe-Piper, G.; Papadopoulou, P.; Bourli, N.; Iliopoulos, G. Depositional Environments and Soft Sediment Deformation in the Early Jurassic Ammonitico Rosso Formation of Western Greece. *Geosciences* **2025**, *15*, 10. https://doi.org/10.3390/geosciences15010010

1. Introduction

The "Ammonitico Rosso" (AR) is a formation (Fm) that developed during the Jurassic period in pelagic environments, and more specifically in swell areas of epioceanic fringes that were widespread in Mediterranean and Alpine regions [1,2]. The AR Fm is one of the best-known lithofacies of the Tethys Ocean's history due to its peculiar lithological features [3]. The main features of the AR Fm are its lithology, characterized by predominant red nodular bedded limestones, and the presence of abundant ammonite (cephalopod) fauna [1]. Additionally, Jenkyns [1] estimated a sedimentation rate for the AR Fm of a few millimetres every thousand years (0.003 mm/year). He also proposed eight main features for the red nodular limestone: (a) the contact between nodules and the matrix is gradational; (b) large microfossils (like juvenile ammonites) are able to cross the matrix–nodule boundary; (c) the matrix exhibits a higher occurrence of skeletal calcite; (d) in certain facies,

a dolomitized matrix is present; (e) microfossils made of silica are preserved only in the nodules; (f) there are either no calcareous nannofossils or they are rare; (g) the nodules seem to have been formed at a very early stage and (h) they do not seem to have been widely deposited since the Upper Jurassic in such nodular limestones. The nodules are magnesium-rich and calcite-rich, soft or hard, with their diameter being commonly of centimetres in scale [1,4]. Thus, they feature a micritic matrix dotted with altered planktonic foraminifera (globigerinids), whereas another characteristic is that the nodules are more calcareous than their matrix. Therefore, nodules must have been formed at or near the sediment–water interface.

The presence of submarine landsliding generally indicates that during sedimentation, the basin floor was inclined, but sliding can take place on extremely mild slopes of 2–3° [5,6], or in a few cases less than 1° [6–8]. Such mass-transport deposits (MTDs) can extend over a range of tens of kilometres and in some cases indicate sites with hydrocarbon prospectivity [6,9]. However, some are limited to a small scale and could influence the migration of hydrocarbons [6,10]. Landslides that produce MTDs occur in loosely consolidated soft sediments in both subaerial and submarine environments [6,8,11–14]. Internal structures in MTDs are likely to indicate the prevailing orientation on the slope during its creation ([12] and references therein). Synsedimentary deformation structures (synsedimentary faults, folds, slide planes, dewatering structures, etc.) are widely distributed in the syn-rift formations of the Ionian Basin of Greece [15,16]. The orientations of these structures indicate that the depositional conditions were influenced by two main factors: the first is related to the opening (extensional stress) of the Pindos Ocean to the east, and the second is halokinesis (evaporites from the base of the Ionian Basin) [17].

2. Geological Setting

The External Hellenides, located along the borders of the Hellenic Arc, are characterized by continuous sedimentation during the Mesozoic, and they underwent tectonism during the main Alpine orogeny [18]. The Ionian Unit consists part of the External Hellenides. They extend (from north to south) to the Ionian Islands, Epirus, Western Sterea, Northwestern Peloponnese, and the Dodecanese Islands (Karpathos and Rhodes) [18]. In central-southern Peloponnese and Crete, the Ionian Basin is represented by its metamorphic equivalent, the Plattenkalk series [19]. The Ionian Basin is bounded by NNW–SSE-directed thrusts, the Gavrovo thrust to the east and the Ionian thrust to the west [15,20], which were active during the Cenozoic Era. From east to west, the Ionian Basin can be subdivided into three sub-basins, internal, middle, and external [20–22] (Figure 1).

During the Mesozoic Era, the Ionian Basin was part of the southeastern passive margins of the Tethys Ocean [20,23,24]. From a palaeogeographical perspective, the Ionian Basin during the latest part of the Early Jurassic was a deep-water basin, which was formed due to the collapse of a pre-existing carbonate platform amid crustal extension, termed as the syn-rift stage [23]. Until the Paleogene, carbonate rocks with argillaceous and siliceous components were deposited, with no significant siliciclastic input [23], in the developing Ionian Basin [17,22,25]. As a result of the rifting, the basin was subdivided into smaller half-grabens [17,22,24], with a north–south orientation of the horsts and grabens. WSW–ENE-directed strike-slip faults acted as transfer faults between different segments of the horsts and grabens. The type and thickness of the sediments and their depositional conditions vary both from east to west and from north to south [22,26–29].

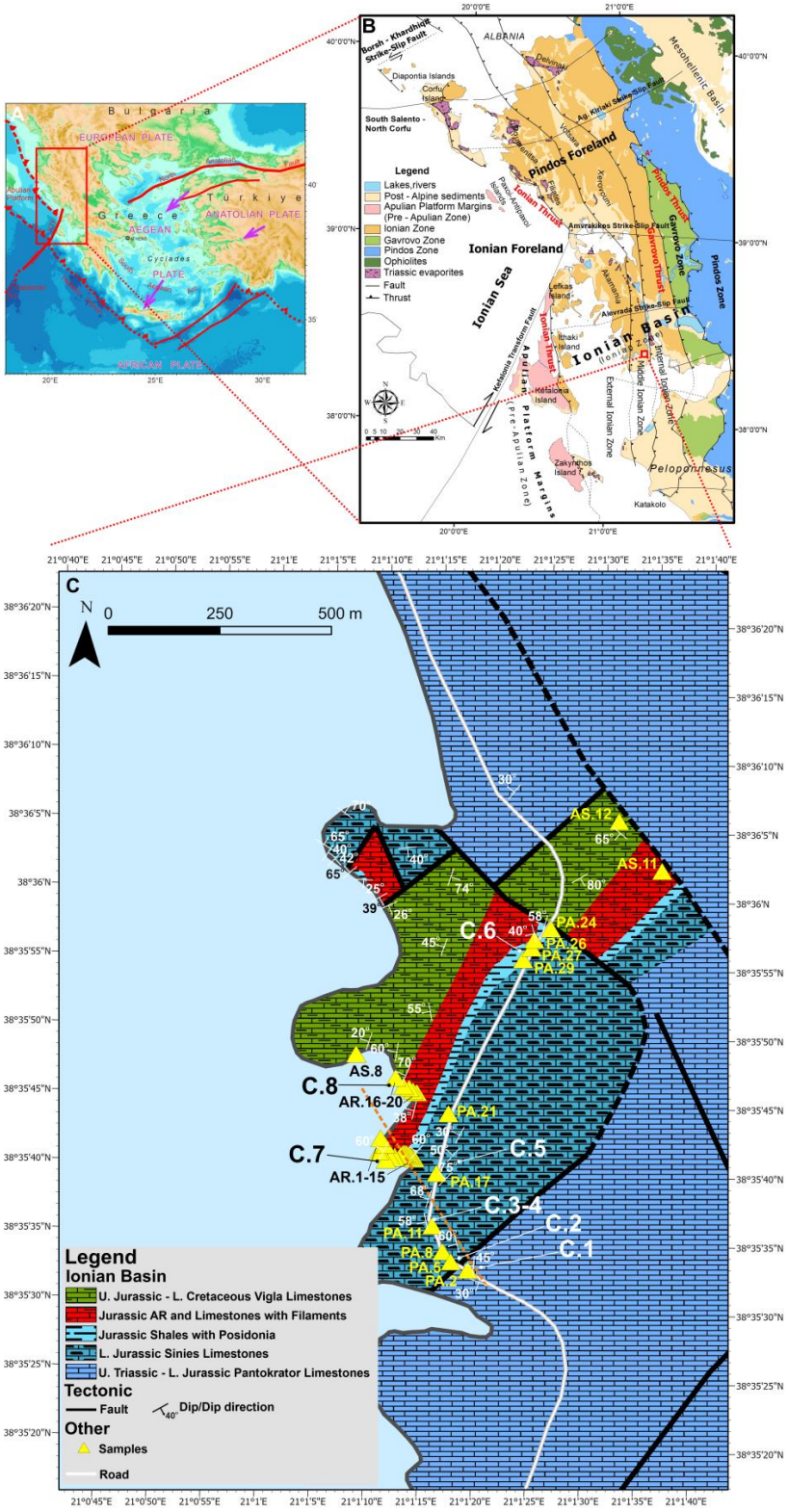

Figure 1. (**A**) Map of Greece, where the red box indicates the location of NW Greece. (**B**) Simplified geological map of the External Hellenides in NW Greece, modified from [22], where the red box indicates the study area. (**C**) Geological map of the study area. The locations of the collected rock samples are also marked. Codes with the letter **C** represent the locations of the stratigraphic columns referred to in the text, while the orange dotted line indicates the position of the cross section in Figure 3A.

In previous studies [17,22,24], the stratigraphic sequences were separated into three stages, the pre-rift, the syn-rift, and the post-rift stages. However, according to recent studies [11,12,15,30,31], the Ionian Basin sequence should be separated into the pre-rift and syn-rift stages. The base of the pre-rift sequence consists of Lower to Middle Triassic evaporites with a total thickness of over 2000 m and the Middle to Upper Triassic Foustapidima Fm limestones (50–150 m thick, black sub-lithographic), overlain by the Lower Jurassic Pantokrator Fm limestones (over 1000 m thick, white massive–thick-bedded) (Figure 2).

The Lower Jurassic–Eocene syn-rift sequence overlies the pre-rift sequence. From the base to the top, the following formations are recognized: (a) Lower Jurassic Sinies Fm limestones (beige pelagic) and the laterally equivalent Louros Fm limestones (hemipelagic, white-light grey medium-bedded) (20–150 m thickness); (b) Lower–Middle Jurassic AR Fm; (c) Middle Jurassic limestones with filaments Fm (bedded) and the laterally equivalent Lower–Upper Jurassic Posidonia bed Fm (Lower and Upper members, yellow-green shaly marly limestones with *Posidonomya*) ranging from a few metres to 200 m thick; in the footwalls of the half-graben sequences, unconformities occur [22] below (d) the Lower–Upper Cretaceous Vigla Fm limestones (beige, pelagic) and the rare Vigla shales (200–600 m thick); (e) Upper Cretaceous Senonian limestone Fm (massive–thick-bedded, neritic); (f) Palaeocene–Eocene limestones with micro-breccia, derived from the erosion of the carbonate rocks of the Gavrovo and Apulian platforms. On top of this syn-rift succession, Middle Eocene–upper Oligocene submarine fans developed in a foreland basin, formed as a response to the compressional regime [13,22,32,33] (Figure 2).

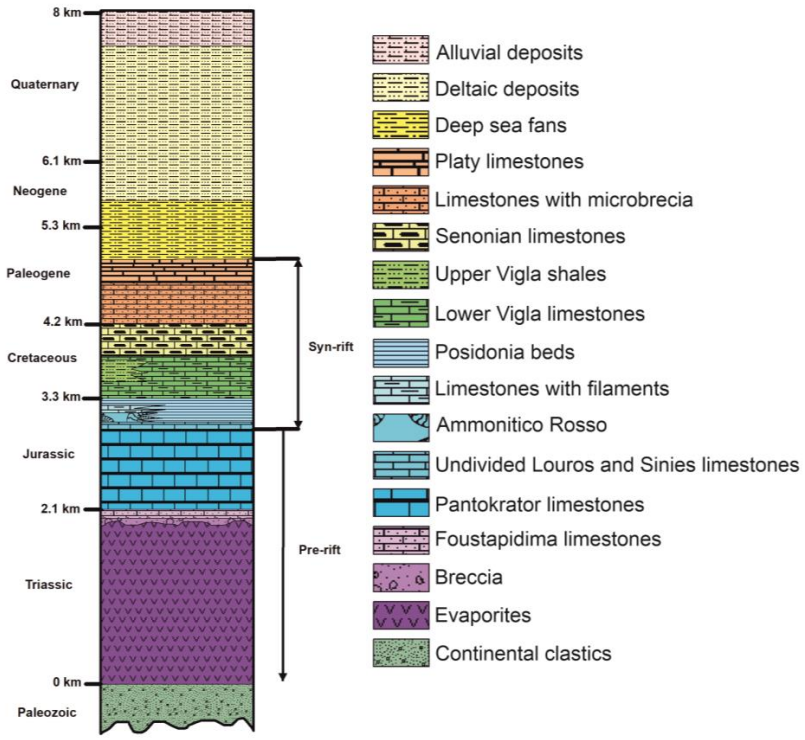

Figure 2. Synthetic lithostratigraphic column of the Ionian Basin (modified from [30,34]).

The aim of this study is to conduct a biostratigraphic and sedimentological determination of the AR Fm in the study area and unravel its internal structure, which includes several horizons of synsedimentary deformation. Additionally, this study examines the transitions from the underlying "Sinies" limestone Fm and the Lower Posidonia bed Fm to the AR Fm, and from the AR Fm to the overlying limestones with filaments and "Vigla" limestone Fms, throughout the Jurassic Period in Western Aitoloakarnania (Western Greece,

External Ionian Zone). Finally, the geological mapping of the studied area was part of this project, which provided a revision of the pre-existing geological map.

The study area is located in the region of Western Greece, in the regional district of Aitoloakarnania, approximately 8 km northwest of Astakos town and 10 km southeast of Mytikas village (Figure 1). In this area, Jurassic and Cretaceous formations of the External Ionian Basin are exposed in coastal sections, road cuts, and sparsely vegetated mountain slopes.

3. Materials and Methods

3.1. Material

In the field, detailed bed-by-bed logs were measured, and then the corresponding lithostratigraphic columns were produced. Fieldwork also included measurements, descriptions, and reconstruction of the studied stratigraphy, bearing in mind the local tectonic activity. A total of 52 rock samples (20 labelled as AR, 29 as PA, and 3 as AS; the labels are related to the formations and sampling locations, with AR for Ammonitico Rosso Fm, PA for Paralia Astakos, and AS for Astakos) were collected from the study area. Thirty of the most characteristic samples were thin-sectioned for microfacies analysis. Thin sections were cut perpendicularly to the bedding. Microfacies analysis was performed using an Optika B-293PLi Microscope (OPTICA Italy, Ponteranica, Italy). X-ray diffraction (XRD) analysis was conducted to determine the lithotypes of the AR limestones, using five different samples (AR.1, AR.6, AR.9, AR.12, and AR.15).

3.2. Methods

The strongly deformed horizons were recorded in detail, including their thickness, deformation axis, their relation to the underlying and overlying horizons, and the bedding planes' dip and direction. Additionally, the characteristics and kinematics of the faults were recorded and analyzed in relation to the depositional processes.

The most commonly used methodologies for carbonate classifications are Folk's [35,36] and Dunham's [37] classifications. The determination and interpretation of carbonate facies are related to lithology, texture, grain size, microfossil assemblages, sediment structures, colour, and diagenetic textures [30,38]. The revised Wilson model [38,39] defines 26 standard microfacies (SMF) types that are associated with 10 standard facies zones (FZ). These facies zones begin from the deep-water basin environment up to the inner platform or to an environment with an intense meteoric influence [40]. Based on the methodologies described above, the thin sections were analyzed to identify and define different microfacies (MF) types, which were then correlated with the previously mentioned SMF types. In thin sections where microfossils were present, a biofacies analysis was conducted, and where possible, the age of the samples was determined. By integrating the results from both biofacies and lithofacies analyses, field observations, and the existing literature, the synthetic stratigraphic column of the study area was constructed. A correlation was also established between the thicknesses of the formations (Pantokrator limestone Fm, Sinies limestone Fm, Posidonia bed Fm, AR Fm, limestones with filaments Fm, and Vigla limestone Fm) identified in this study and those reported in previous studies of the same formations at other locations.

X-ray diffraction was used for the determination of mineral phases (Bruker D8 Advance, USA (Bruker Corporation, Billerica, MA, USA), with Ni-filtered CuKα radiation, equipped with a LynxEye®detector and Autochanger system (Bruker Corporation, Billerica, MA, USA), including a rotating sample stage). For the evaluation of the obtained diffractograms, DIFFRACplus EVA software was used (Bruker-AXS, Madison, WI, USA),

based on the ICDD Powder Diffraction File (2006 version). The scanning area covered the 2θ interval 2–70°, with a scanning angle step size of 0.015° and a time step of 0.1 s.

4. Results

4.1. Field Decriptions

The Jurassic to Cretaceous formations of the External Ionian sub-basin were studied, focusing on the AR Fm, as it appears fully developed in the study area. Specifically, in this area, the following formations are exposed (from the base to the top): Pantokrator limestones, Sinies limestones, Lower Posidonia beds, AR, limestones with filaments, and Vigla limestones (Figure 3). The base of the succession consists of massive- to thick-bedded white limestones (Pantokrator Fm). These are overlain by thin- to medium-bedded siliceous limestones (Sinies Fm) which locally contain ichnofossils, stylolites, and occasional chert nodules. Conformably, on the latter, alternations of laminated green-brown pelites with laminated marly limestones were recognized (possible Posidonia beds). Above them, alternations of red pelites and calcilutites with grey and red nodular limestones were observed (AR Fm). In the red pelites, grey nodular limestones, and red nodular limestones, ammonites and ichnofossils were observed. The upper stratigraphic part of this formation consists of pink-beige limestones (limestones with filaments Fm). These strata are laminated to medium-bedded. In the upper part of the studied section, thin- to thick-bedded beige siliceous limestones with chert nodules and chert bands (Vigla limestone Fm) are present. Notably, within this upper formation, brown shales containing very small polymetallic nodules were recorded.

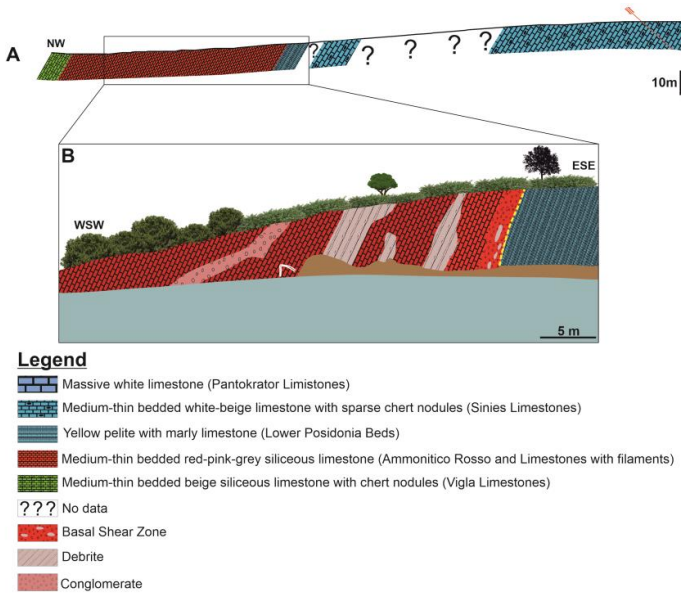

Figure 3. (**A**) Geological section of the studied area, and (**B**) close-up view of the second section, providing details of the slumped AR Fm. The yellow dotted line represents the transition from the Posidonia bed Fm to the basal shear zone of the AR Fm.

The bedding planes show a predominantly northwest direction, while their dip angles vary from 20° to 68°. Additionally, reverse and normal faults were observed, both dipping southeastwards but with different angles (330°/68°, 236°/48°) (Figure 1).

4.2. Facies Analysis and Zones

Of a total of 30 studied thin sections, two different depositional environments (toe of slope and platform-margin reefs) were recognized, corresponding to two different standard microfacies types (with two sub-types). Each MF corresponds to a different SMF type. Specifically, MF

1 is classified as biosparite/boundstone, while MF 2 includes micrites, fossiliferous micrites, and both sparse and packed biomicrites/wackestones and packstones (Table 1).

Table 1. Summarized table of determined microfacies types with their main lithological features.

MF	SMF Type	FZ	Description	Samples
1	7	5	Unsorted biosparite/boundstone	PA.2
2	3	3	Sparse and fossiliferous micrite, micrite/wackestone–mudstone	PA.5, PA.8, PA.11, PA.17, PA.21, PA.24, PA.29, AR.1, AR.2, AR.3, AR.5, AR.6, AR.7, AR.10, AR.14, AR.16, AR.18, AR.20
	3-RAD	3	Packed biomicrite/wackestone–packstone	AS.8
	3-CALP	3	Packed biomicrite/wackestone	AS.12
	3-FIL	3	Sparse to packed biomicrite/ wackestone–packstone	AS.11, AR.8, AR.9, AR.11, AR.12, AR.13, AR. 15, AR.17, AR.19

4.2.1. MF 1

Thin section PA.2 was classified as unsorted biosparite, according to Folk's classification, and as boundstone, according to Dunham's classification (Figure 4A). The presence of micro-fractures, filled mainly with calcite and to a lesser extent with bitumens, was observed. The porosity is fenestral, and geopetal structures and ooids were noted. *Thaumatoporella* J. Pia, 1927 was found. This microfacies can be characterized as SMF type 7. Thus, this type shows that the deposition took place in platform-margin reefs (FZ 5, according to Wilson's model).

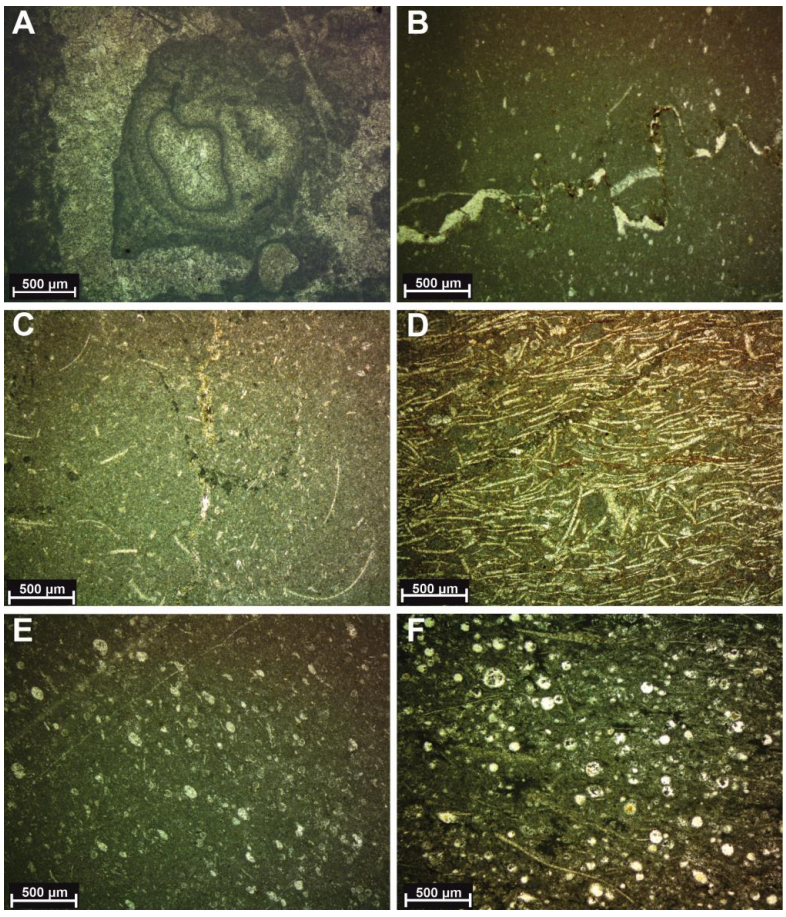

Figure 4. Representative images from each SMF type: (**A**) sample PA.2 (SMF 7), indicating an unsorted biosparite/boundstone; (**B**) sample PA.29 (SMF 3), representing a fossiliferous micrite/wackestone;

(**C**) sample AR.14 (SMF 3), depicting a packed biomicrite/packstone; (**D**) sample AR.12 (SMF 3-FIL), indicating a packed biomicrite/packstone with filaments; (**E**) sample AS.12 (SMF 3-CALP), representing a packed biomicrite/wackestone with calpionellids; (**F**) sample AS.8 (SMF 3-RAD), depicting a packed biomicrite/wackestone–packstone with Radiolaria.

4.2.2. MF 2

This microfacies includes micrites, fossiliferous micrites, and both sparse and packed biomicrites, based on Folk's classification, and wackestones and packstones, according to Dunham's classification. So, the majority of the studied samples were determined as SMF type 3, and more specifically the sub-types SMF-3FIL, SMF-3CALP, and SMF-3RAD (because they contain many bivalves, calpionellids, and Radiolaria, respectively).

Samples PA.5, PA.8, PA.11, PA.17, PA.21, PA.24, PA.29 (Figure 4B), AR.1, AR.2, AR.3, AR.5, AR.6, AR.7, AR.10, AR.14 (Figure 4C), AR.16, AR.18, and AR.20 were classified as sparse biomicrites, fossiliferous micrites, and micrites based on Folk's classification, while based on Dunham's classification, they can be described as wackestones and mudstones. Stylolites with low-amplitude peaks were observed mainly parallel to the bedding. In all of the studied thin sections, micro-fractures filled with calcite were present. Bitumen traces with low to very low contents and a few metallic oxides were found. The bitumens sometimes fill the secondary microporosity, while both bitumens and oxides are occasionally present in stylolites and micro-fractures. Several samples have undergone intense recrystallization. This microfacies can thus be characterized as the SMF-3 type and represents deposition that took place at the toe of a slope (FZ 3, according to Wilson's model).

Sample AS.8 was classified as packed biomicrite (Folk's classification) and as wackestone to packstone (Dunham's classification). The bitumen content is low to medium, filling the microporosity and also occurring in stylolites. Radiolaria (both Spumellaria and Nassellaria), planktonic foraminifera of the genus *Globigerinelloides* Cushman & Ten Dam, 1948, sponge spicules, and bioclasts were identified. The presence of a sparse number of Radiolaria led to a classification of the SMF 3-RAD microfacies type, which was also deposited at the toe of a slope (FZ 3, according to Wilson's model).

The thin section of AS.12 was classified as packed biomicrite (Folk's classification) and as wackestone (Dunham's classification). Low bitumen content was observed filling the secondary porosity, along with calcite-filled fractures. Stylolites with peaks of low amplitude with metallic oxides on their edges were observed; however, these oxides were also found to be scattered. The fossils present are ammonite aptychi, calpionellids, Radiolaria, and bioclasts. The presence of calpionellids is indicative of the SMF 3-CALP type, which characterizes a deep-sea environment (FZ 3, based on Wilson's model).

Samples S.11, AR.8, AR.9, AR.11, AR.12 (Figure 4D), AR.13, AR. 15, AR.17, and AR.19 were classified as sparse to packed biomicrites (Folk's classification) and as wackestones–packstones (Dunham's classification). Stylolites with low-amplitude peaks were observed mainly parallel to the bedding and rarely perpendicular to this. Fractures filled with calcite were found. Also, scattered bitumens with low to very low contents were traced, sometimes filling the secondary porosity, sometimes in micro-fractures, and sometimes in the stylolite voids. Metallic oxides were mainly found scattered and occasionally found in micro-fractures and stylolites. The fossils in these samples included mainly filaments (densely packed), ammonites (and aptychi), Radiolaria, and ostracods. In many samples, planktonic and benthic foraminifera, corals, gastropods, and several bioclasts were observed. The extensive presence of filaments, as described above and seen in Figure 4D, indicates the SMF 3-FIL type, suggesting that deposition also took place at the toe of a slope (FZ 3, according to Wilson's model).

4.3. Lithostratigraphy and Biostratigraphy of the Study Area

For each part of the study area bounded by a tectonic discontinuity, an individual lithostratigraphic column of each sequence was constructed, showing the locations of the samples and the resulting lithofacies interpretation and key microfossils. Four samples are not related to a specific column, and for one of them, there is a schematic drawing of the respective section.

Sequence 1 consists of massive white limestones, where sample PA.2 was collected from. According to the biofacies analysis, bivalve filaments and *Thaumatoporella* sp. J. Pia, 1927 were found. These taxa indicate a shallow marine/shallow-shelf environment of deposition. Hitherto, this biofacies is indicative of the Pantokrator limestone Fm (Figure 5).

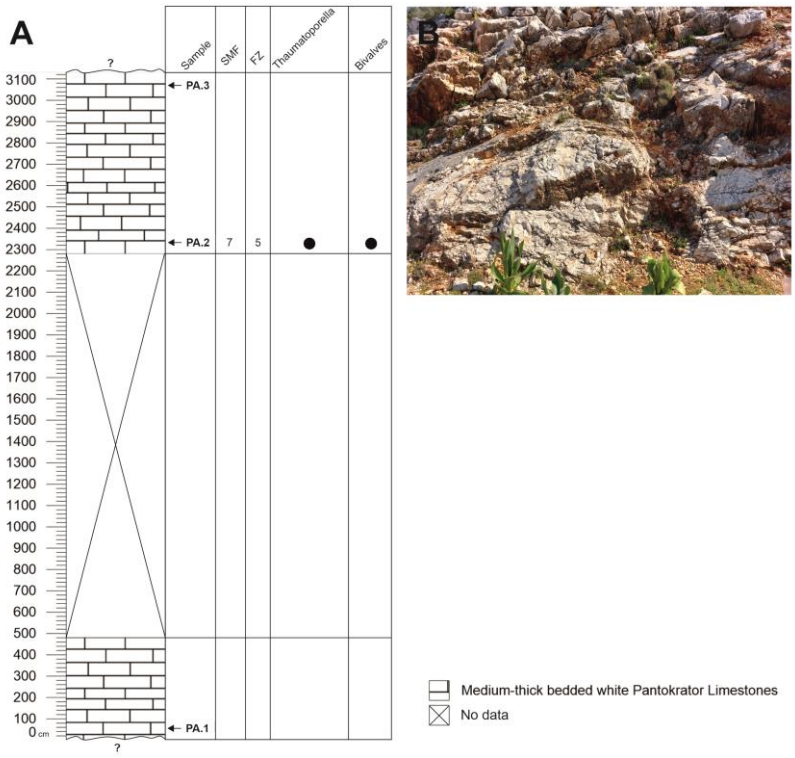

Figure 5. (**A**) Stratigraphic column of sequence 1 (C.1) with the occurrences of fossil taxa that have been found. See Figure 1 for the position of the column of this sequence. (**B**) Representative photo of the outcrop section of C.1.

Sequence 2 (Figure 6), from the base to the top, consists of medium–thick-bedded beige limestones, thick-bedded beige limestones with chert nodules (trace fossils were found as well), thin–medium-bedded beige limestones with chert nodules, thick-bedded beige limestones with sparse chert nodules, and medium-bedded beige limestones. Rock samples PA.5 and PA.8 were collected from this sequence. In thin section PA.5, benthic foraminifera and ammonites were found, while in PA.8, Radiolaria and gastropods were found. The above-described lithologies are characteristics of the Sinies limestone Fm.

Sequences 3 and 4 consist of marly limestones containing Radiolaria and ammonites. They are characterized by thin-bedded pelagic limestones, with Posidonia beds as the overlying Fm and the Pantokrator Fm as the underlying Fm. Therefore, their stratigraphic position indicates that they possibly belong to the Sinies limestone Fm (Figure 7). Sample PA.11 was collected from sequence 3.

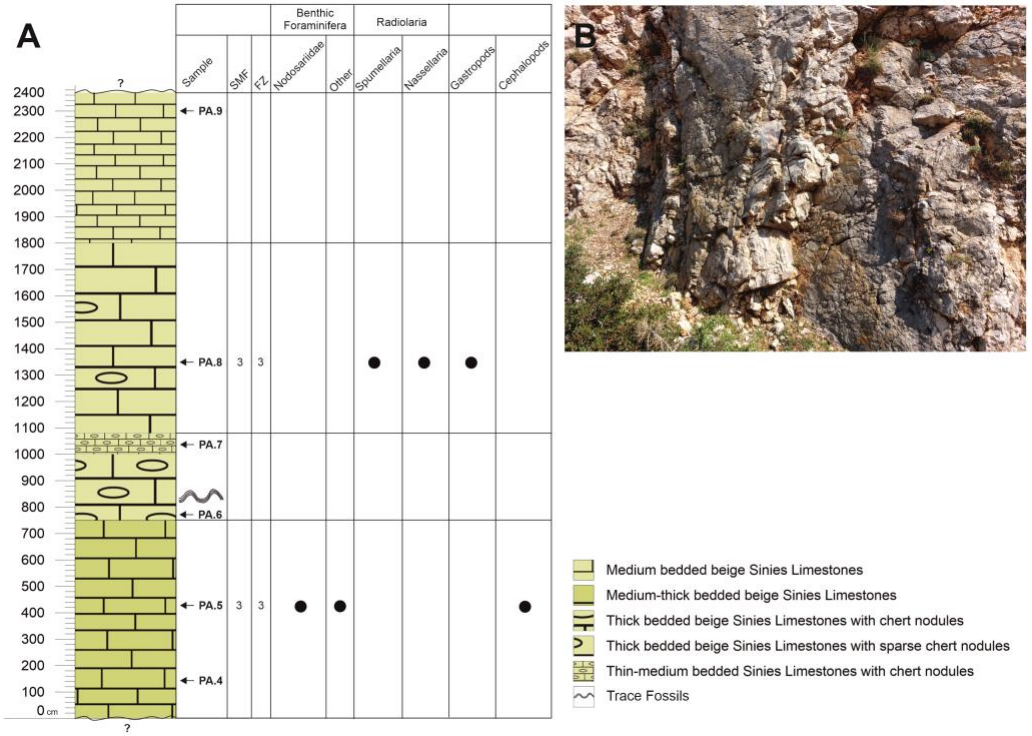

Figure 6. (**A**) Stratigraphic column of sequence 2 (C.2) with the occurrences (black dots) of each fossil taxon that has been found. See Figure 1 for the position of the column of this sequence. (**B**) Representative photo of the outcrop section of C.2.

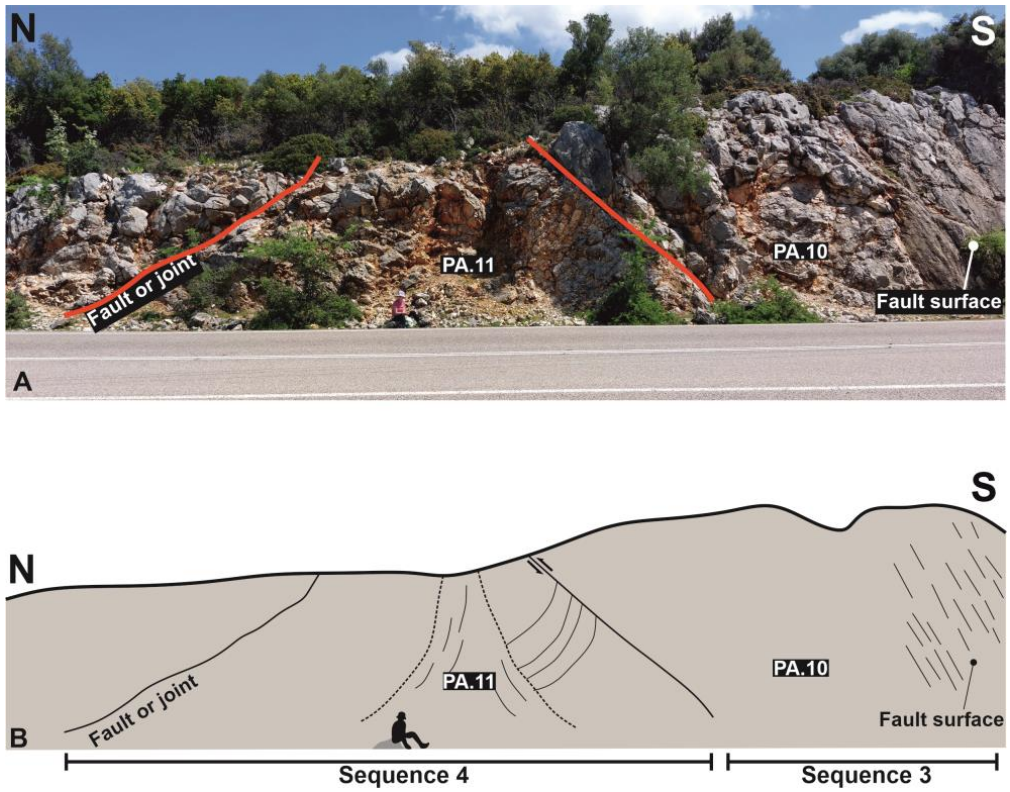

Figure 7. The section where sequences 3 (sample PA.10) and 4 (sample PA.11) are outcropping (**A**), and the corresponding schematic drawing which provides a better visualization of the tectonic discontinuities that interrupt the two sequences (**B**), where samples PA.10 and PA.11 were collected from. See Figure 1 for the respective position of this outcrop on the map.

From the base to the top, the following lithologies are present in sequence 5 (Figure 8), where samples PA.17 and PA.21 were collected from: medium-bedded marly limestones with chert nodules, thin–medium-bedded limestones with chert nodules, limestones with micro-breccia and clasts, medium-bedded marly limestones with chert nodules (with trace fossils), thin–medium-bedded siliceous limestones, and thin–thick-bedded limestones with chert bands and trace fossils. In sample PA.17, the planktonic foraminifera *Globuligerina* cf. *glinskikhae* Gradstein & Waskowska 2021 (Figure 9A) and *Globuligerina* sp. Bignot & Guyader 1971 and Radiolaria were found. In sample PA.21, the planktonic foraminifera *Globuligerina* sp. Bignot & Guyader 1971 (Figure 9B) and benthic foraminifera were found. Based on a recent study of planktonic foraminifera [41], the first occurrence of some *Globuligerina* Bignot & Guyader 1971 species is the Toarcian. However, as these samples belong to the upper part of Sinies limestone Fm, based on their lithological features (bedded neritic limestones) and their relationship to the overlying formations (the overlying Fm is Posidonia beds) (Figure 1), they appear to have been deposited during the Late Pliensbachian. If verified, this claim would shift the first appearance of planktonic foraminifera from the Toarcian to the Pliensbachian.

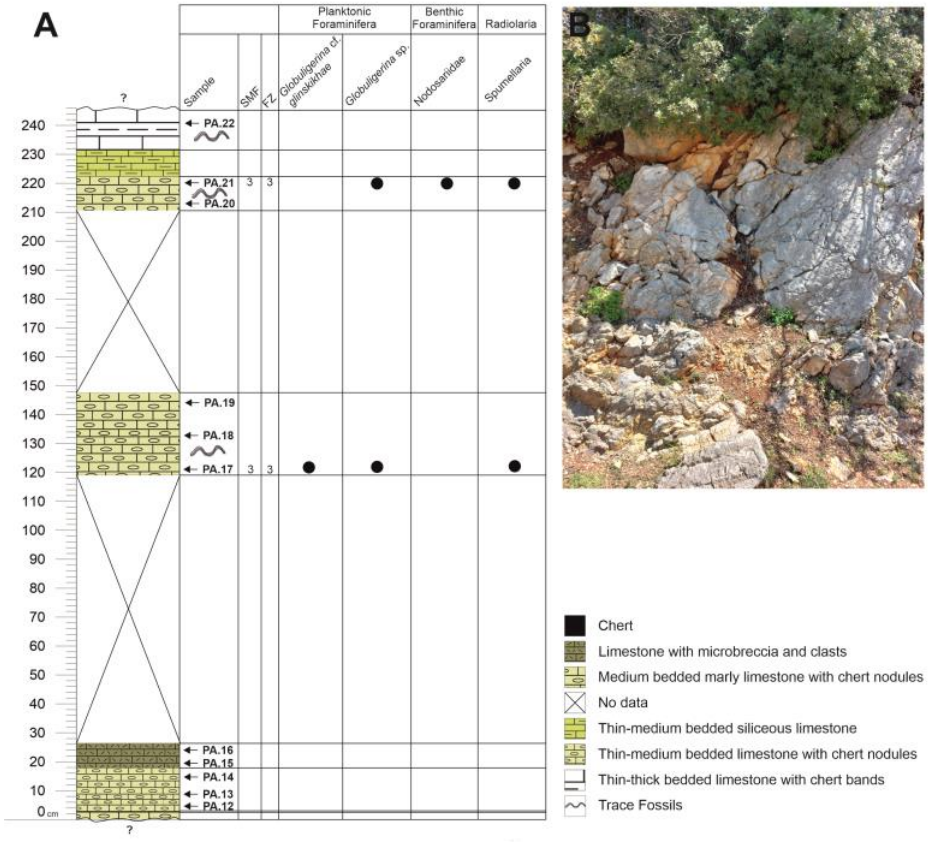

Figure 8. (**A**) Stratigraphic column of sequence 5 (C.5) with the occurrences (black dots) of each microfossil taxon that has been found. See Figure 1 for the position of the column of this sequence. (**B**) Representative photo of the outcrop section of C.5.

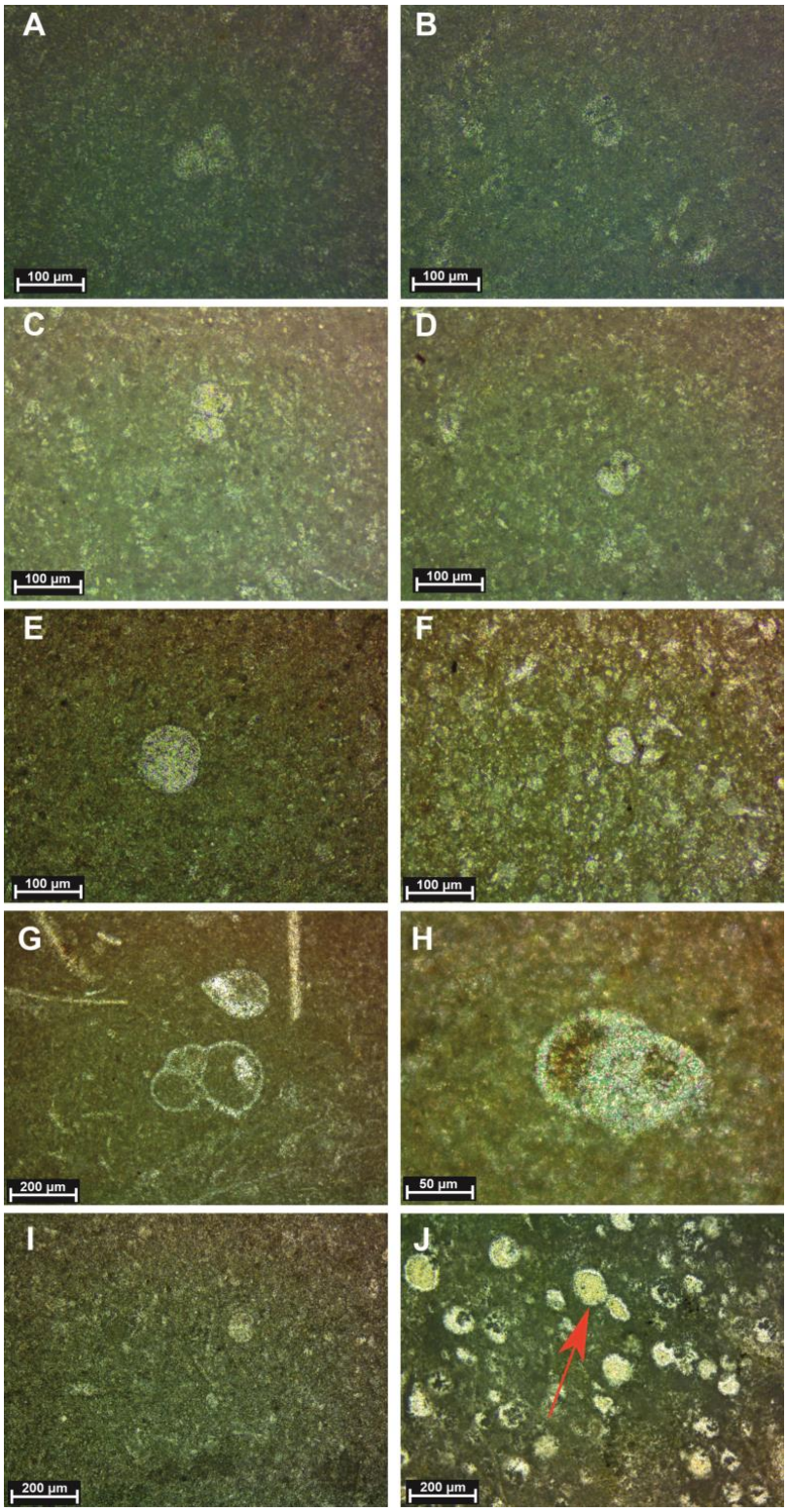

Figure 9. Representative microphotographs of planktonic foraminifera (**A**) *Globuligerina* cf. *glinskikhae* Gradstein & Waskowska 2021 (sample PA.17), (**B**) *Globuligerina* sp. Bignot & Guyader 1971 (sample PA.21), (**C**) *Globuligerina* sp. Bignot & Guyader 1971 (sample PA.24), (**D**) *Globuligerina glinskikhae* Gradstein & Waskowska 2021 (PA.24), (**E**) *Globuligerina* cf. *glinskikhae* Gradstein & Waskowska 2021 (sample AR.5), (**F**) *Globuligerina oxfordiana* (Grigelis, 1958) (sample AR.15), (**G**) *Globuligerina oxfordiana* Grigelis, 1958 (sample AR.11), (**H**) *Globuligerina* cf. *oxfordiana* (Grigelis, 1958) (sample AR.11), (**I**) *Globuligerina oxfordiana* Grigelis, 1958 (sample AR.18), and (**J**) *Globigerinelloides blowi* Bolli, 1959, red arrow (sample AS.8).

From the base to the top, sequence 6 (Figure 10) consists of thin–medium-bedded limestones with chert nodules and bands, marly limestones, blue pelites with carbonate nodules, beige calcitic marls, marly limestones, pelites, marly limestones (with trace fossils), blue pelites with carbonate nodules, marly limestones, beige pelites, alternations of marly limestones and blue pelites with carbonate nodules, beige calcitic marls, and brown-yellow pelites. Samples PA. 24 and PA.29 were collected from this sequence. *Globuligerina* sp. Bignot & Guyader 1971 and *Globuligerina glinskikhae* Gradstein & Waskowska 2021 (Figure 9C and D, respectively), as well as Radiolaria, were found in sample PA.24. Based on a recent study on planktonic foraminifera [41], the first occurrence of some *Globuligerina* Bignot & Guyader 1971 species is the Toarcian. Nevertheless, based on their lithological features and relationship to the overlying formation, the AR Fm (Figure 1), these samples belong to the upper part of the Sinies limestone Fm. Thus, these samples were deposited during the Upper Pliensbachian. The second sample (PA.29) contained the following fossil taxa: benthic foraminifera, Radiolaria, and bivalve filaments. None of these taxa are suitable for possible age determinations.

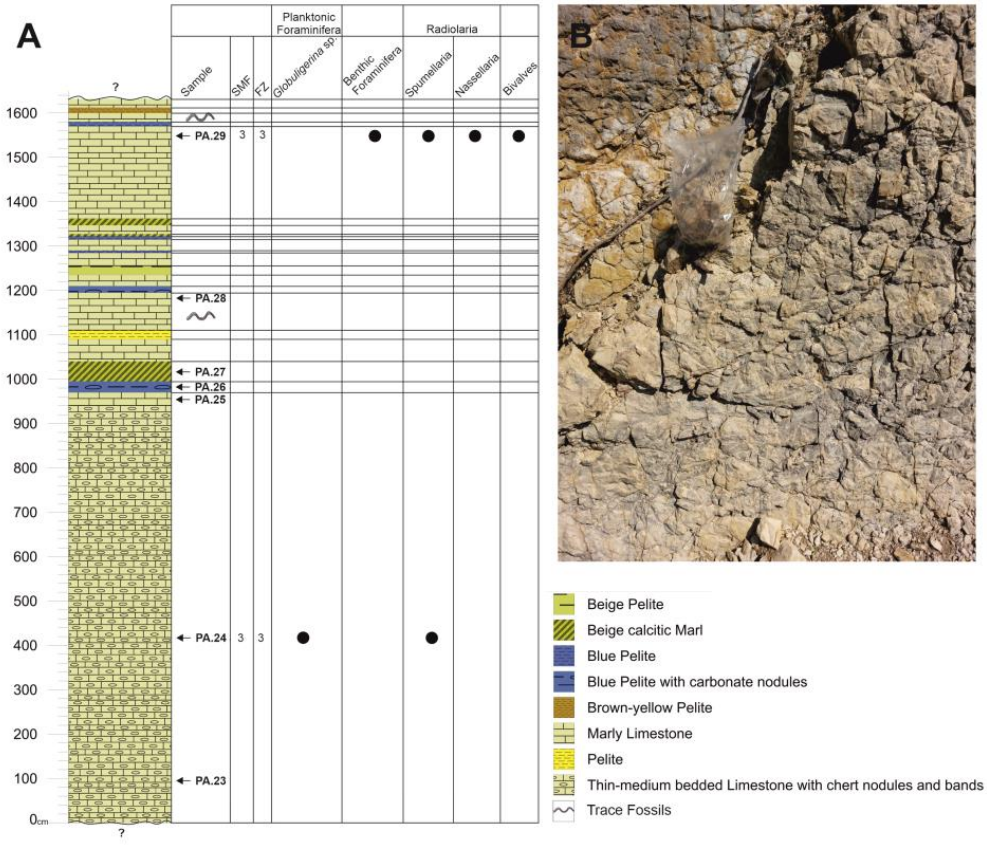

Figure 10. (**A**) Stratigraphic column of sequence 6 (C.6) with the stratigraphic occurrences (black dots) of each fossil taxon that has been found. See Figure 1 for the position of the column of this sequence. (**B**) Representative photo of the outcrop section of C.6.

In a separate study by Golfinopoulos et al. [42] on the benthic microfauna found in the pelites of the upper part of sequence 6, benthic foraminifera and ostracod species assemblages were recorded in samples PA.26 and PA.27, suggesting that they accumulated in an outer-shelf marine environment, characterized by normal salinity, low energy levels in soft sediments, sufficient nutrients, and high levels of dissolved oxygen.

Two samples from the Vigla limestone Fm were examined, one outcropping on the coast and the second one close to a highway (Figure 1). Sample AS.11 is a red siliceous limestone, and Radiolaria, bivalve filaments, gastropods, and ammonites were found, while

sample AS.12 is a beige siliceous limestone, and the calpionellids *Calpionella alpina* Lorenz, 1902 and *Calpionella grandalpina* Nagy, 1986 (Figure 4E), Radiolaria, and ammonites were found. Thus, based on the calpionellid biozonation from [43], the age of the second sample is the late Tithonian.

Sequence 7, from the base to the top (Figures 11 and 12), consists of beige marly limestones with metallic oxides; alternations of yellow-green pelites (occasionally with carbonate nodules), green pelites (occasionally with carbonate nodules and pebbles), beige limestones, and grey marly limestones; and alternations of red limestones, red calcilutites (occasionally nodular), red nodular–brecciated limestones, red pelites, and pink-beige and grey-red limestones. At the top of this sequence, grey calcilutites are developed, together with grey pelites and grey (nodular or marly at times) limestones. Interestingly, synsedimentary deformation structures were observed in this succession, and their features will be analyzed below (see Section 4.4). A micropalaeontological study of the clastic sediments has already been conducted [42] (samples AR.4, AR.6A, AR.7A, AR.7B, AR.9A, and AR.10A). Microfacies analysis of the respective limestones is reported in Section 4.2 and Table 1 (samples AR.1–3 and AR.5–15). For the age determination of Jurassic sequences, it is important to recover planktonic foraminifera. In three of the samples (AR.5, AR.11, AR.15), planktonic foraminifera were found. In sample AR.5, the presence of *Globuligerina* cf. *glinskikhae* Gradstein & Waskowska 2021 (Figure 9E) indicates an age up to the Bathonian [41]. In samples AR.11 and AR.15, the presence of *Globuligerina oxfordiana* Grigelis, 1958 (Figure 9G, H, and F, respectively) suggests a Bajocian to early Tithonian age [41]. In the thin sections of this sequence, planktonic foraminifera (*Globuligerina* species Bignot & Guyader 1971), benthic foraminifera (Lagenidae, Nodosariidae, Archaediscidae, *Lenticulina* Lamarck, 1804, and other taxa which were not determined), crinoids, Radiolaria (both Spumellaria and Nassellaria), bivalve filaments, ostracods, and ammonites were recorded. During field work and logging, trace fossils were found in grey-red limestones, and ammonites were present in red pelites, red limestones, and grey nodular limestones. In grey nodular limestones and beige marly limestones, metallic oxides were also found.

Sample AR.4 consists of clastic sediments, and a micropalaeontological study revealed benthic foraminifera, ostracod moulds, echinoderm spines and spine bases, and one fish tooth. Identification of the ostracod moulds was not possible due to their preservation condition. The most abundant benthic foraminifera taxa of the assemblage are *Eoguttulina* Cushman & Ozawa, 1930 and *Prodentalina* Norling, 1968. Species of the genera *Lenticulina* Lamarck, 1804, *Lagena* Walker and Boys, 1798, *Nodosaria* Lamarck, 1816, and *Lagenamina* Rhumbler, 1911 are also present. Also, possibly broken *Bositra* Gregorio, 1886 shells were found. Thus, based on the living conditions of the identified benthic foraminifera in this sample, these assemblages show that they had developed in the deepest part of the outer shelf where turbidites or slumps could develop. Taxa that inhabited inner- to middle-shelf environments seem to have been transported to the outer shelf. The salinity was normal, and the waters were well oxygenated with high levels of nutrient supply [43] and references therein. Samples AR.6A, AR.7A, and AR.7B represent assemblages similar to sample AR.4 [42]. Sample AR.6A consists of benthic foraminifera, a few sea urchin spines, and broken bivalves. The dominant genus is *Prodentalina* Norling, 1968, while *Lenticulina* Lamarck, 1804, and *Vaginulina* are present in very small numbers of individuals. Sample AR.7A includes benthic foraminifera, ostracod moulds, and echinoid spines, as well as broken bivalves and fish teeth. The dominant genera are *Prodentalina* Norling, 1968 and *Lenticulina* Lamarck, 1804, while small numbers of individuals of *Vaginulina* d'Orbigny, 1826 and *Nodosaria* Lamarck, 1816 were found. Sample AR.7B consists of benthic foraminifera, ostracod moulds, and broken bivalves. Only *Prodentalina* Norling, 1968 species were found.

These samples indicate transport from a shallower to a deeper depositional environment. Samples AR.9A and AR.10A were barren.

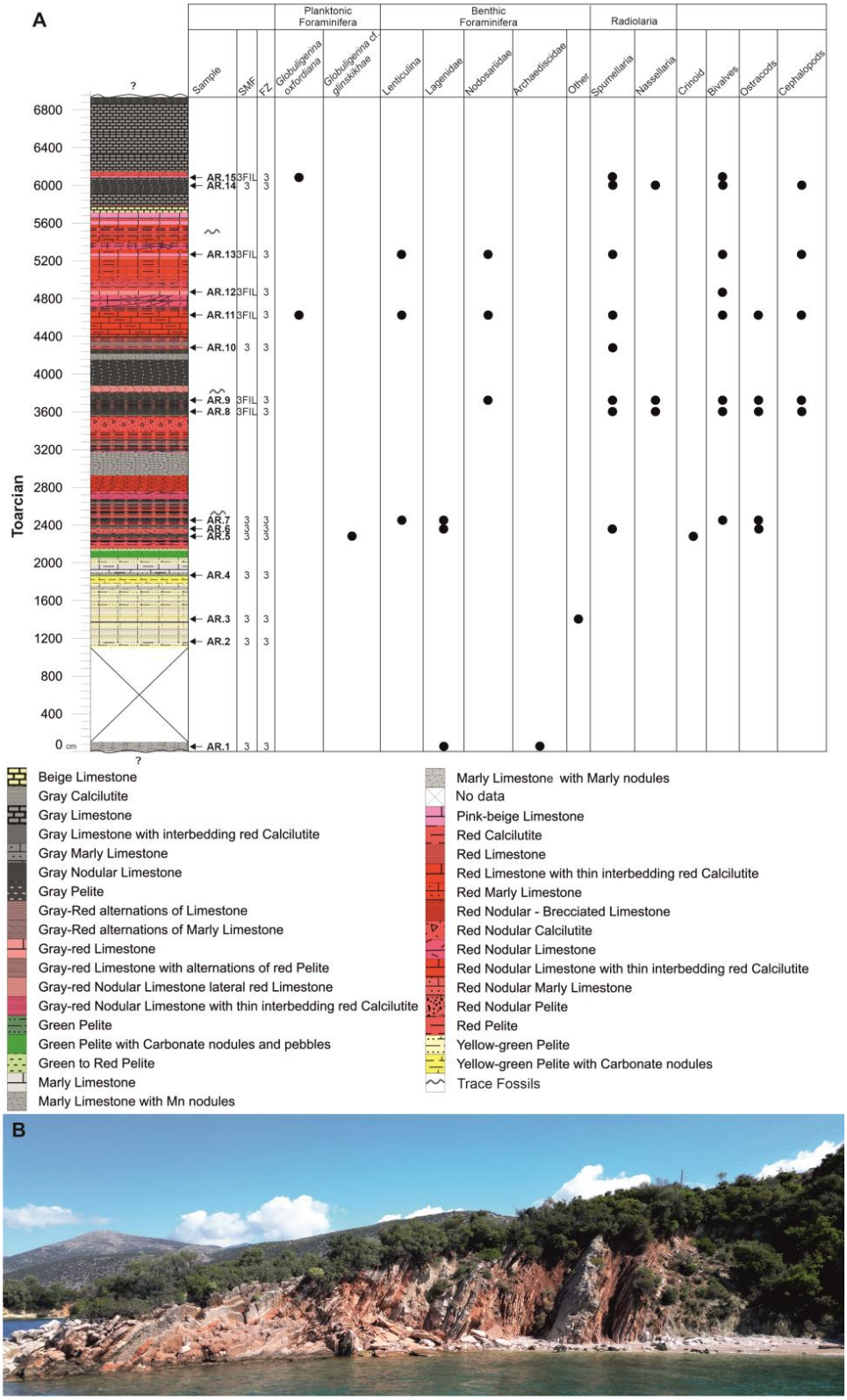

Figure 11. (**A**) Stratigraphic column of sequence 7 (C.7) with stratigraphic occurrences (black dots) of each fossil taxon that has been found. See Figure 1 for the position of the column of this sequence. (**B**) Representative photo of the outcrop section of C.7.

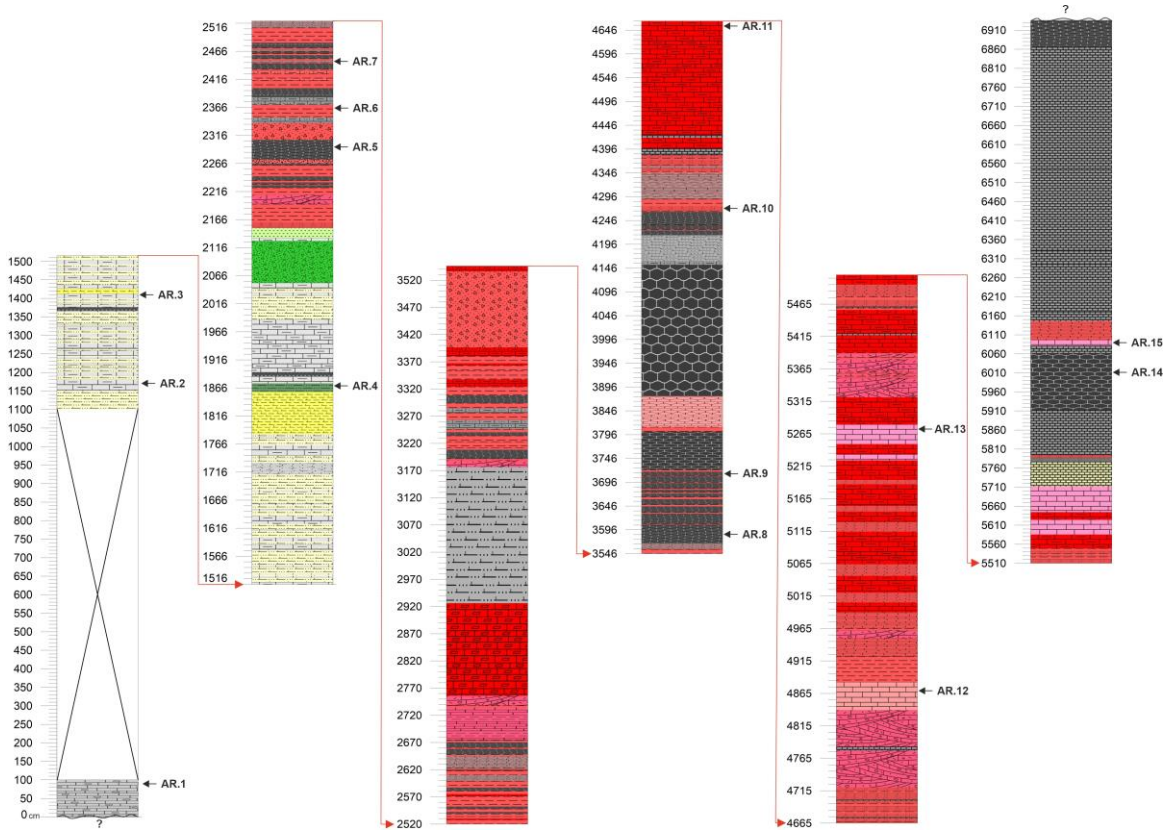

Figure 12. For a more detailed description, the stratigraphic column of sequence 7 is presented in shorter segments and higher analysis. For the lithology symbols, see Figure 11A.

Sequence 8 (Figure 13) represents a layer succession from a coastal section belonging to the Vigla limestone Fm. From the base to the top, the sequence consists of beige marly limestones, cherts, beige brecciated limestones, brown shales, bedded beige limestones, beige brecciated limestones, brown shales, beige siliceous limestones, bedded beige limestones, cherts, and beige siliceous limestones. Samples AR.16–20 were collected from this sequence. Index fossils were found only in one sample (AR.18). These fossils are *Globuligerina oxfordiana* Grigelis, 1958 (Figure 9I) and *Calpionella alpina* Lorenz, 1902, indicating deposition during the Tithonian and confirming the identification of these limestones as belonging to the Vigla Fm. In the five studied samples of this sequence, in addition to the above-mentioned taxa, the following fossil taxa were found: benthic foraminifera (*Bolivina* d'Orbigny, 1839, *Lituonella* Schlumberger, 1905, and Nodosariidae), Radiolaria (both Spumellaria and Nassellaria), bivalve filaments, ammonites, corals, and algae (Figure 13).

Sample AS.8 stratigraphically overlies AR.20; nevertheless, it is not included in the column of sequence 8, as it is located more than 20 m above the top of sequence 8. *Globigerinelloides blowi* Bolli, 1959 (Figure 9J) tests were found, indicating a Barremian to Aptian age [44]. This is a sequence of beige thin-bedded pelagic limestones, and thus these rocks are also considered part of the Vigla limestone Fm.

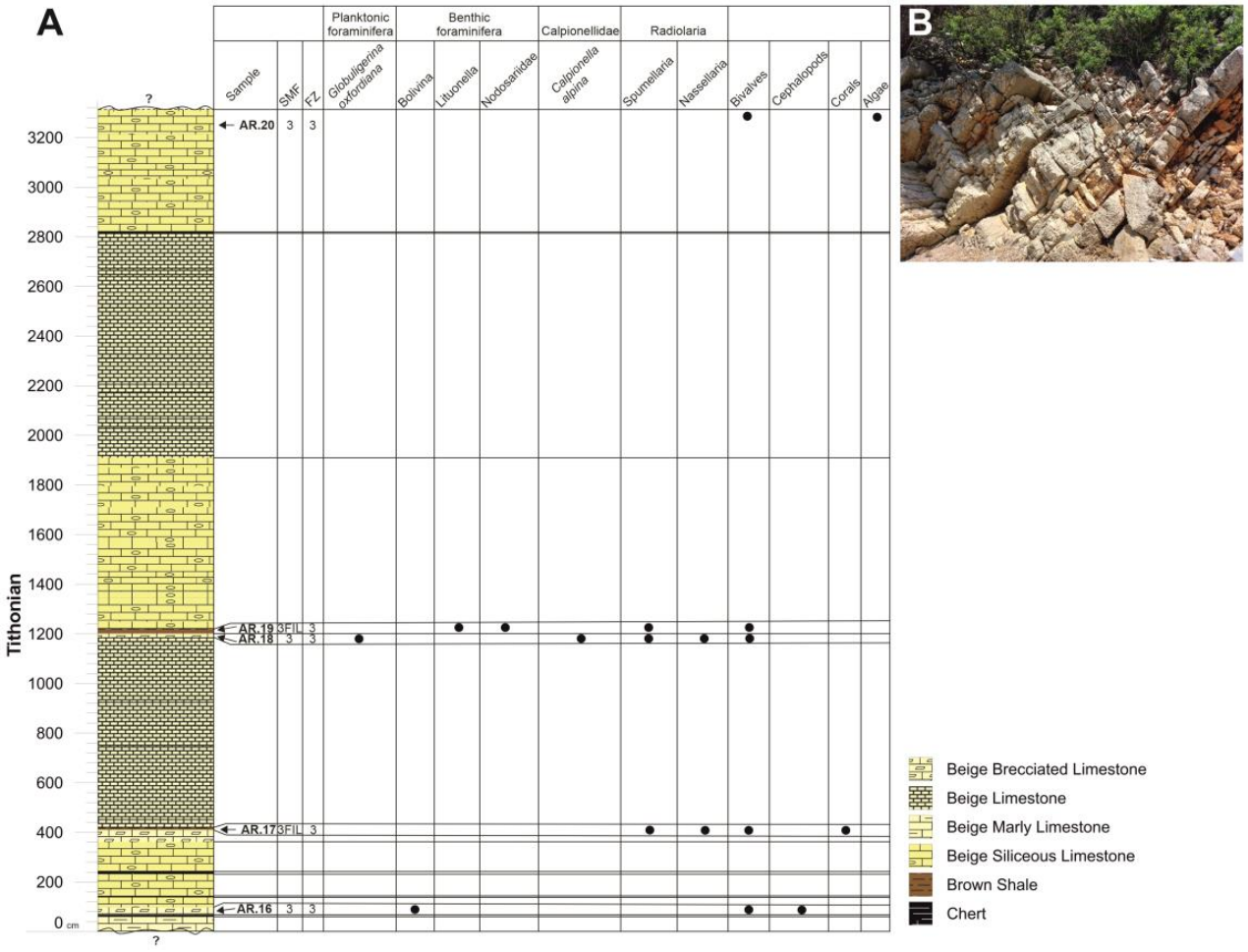

Figure 13. (**A**) Stratigraphic column of sequence 8 (C.8) with the stratigraphic occurrences (black dots) of the determined fossil taxa. See Figure 1 for the position of the column of this sequence. (**B**) Representative photo of the outcrop section of C.8.

4.4. Correlations of Lithostratigraphic Columns

According to the above biostratigraphic and lithological data, the correlations of the studied columns with the synthetic lithostratigraphic column of the Ionian Zone are shown in Figure 14. More specifically, column 1 constitutes the upper part of the Pantokrator Fm limestones, column 2 the lower part of the Sinies Fm limestones, and column 5 the intermediate part of the Sinies Fm limestones. Column 6 constitutes the upper part of the Sinies Fm limestones, as well as the Lower Posidonia bed Fm. Column 7 begins with the uppermost part of the Sinies Fm limestones; stratigraphically higher are the Lower Posidonia Fm beds, where they overlay with the AR Fm, and at the top is the limestones with filaments Fm. Finally, column 8 consists of the upper part of the limestones with filaments Fm and the lower part of the Vigla Fm limestones.

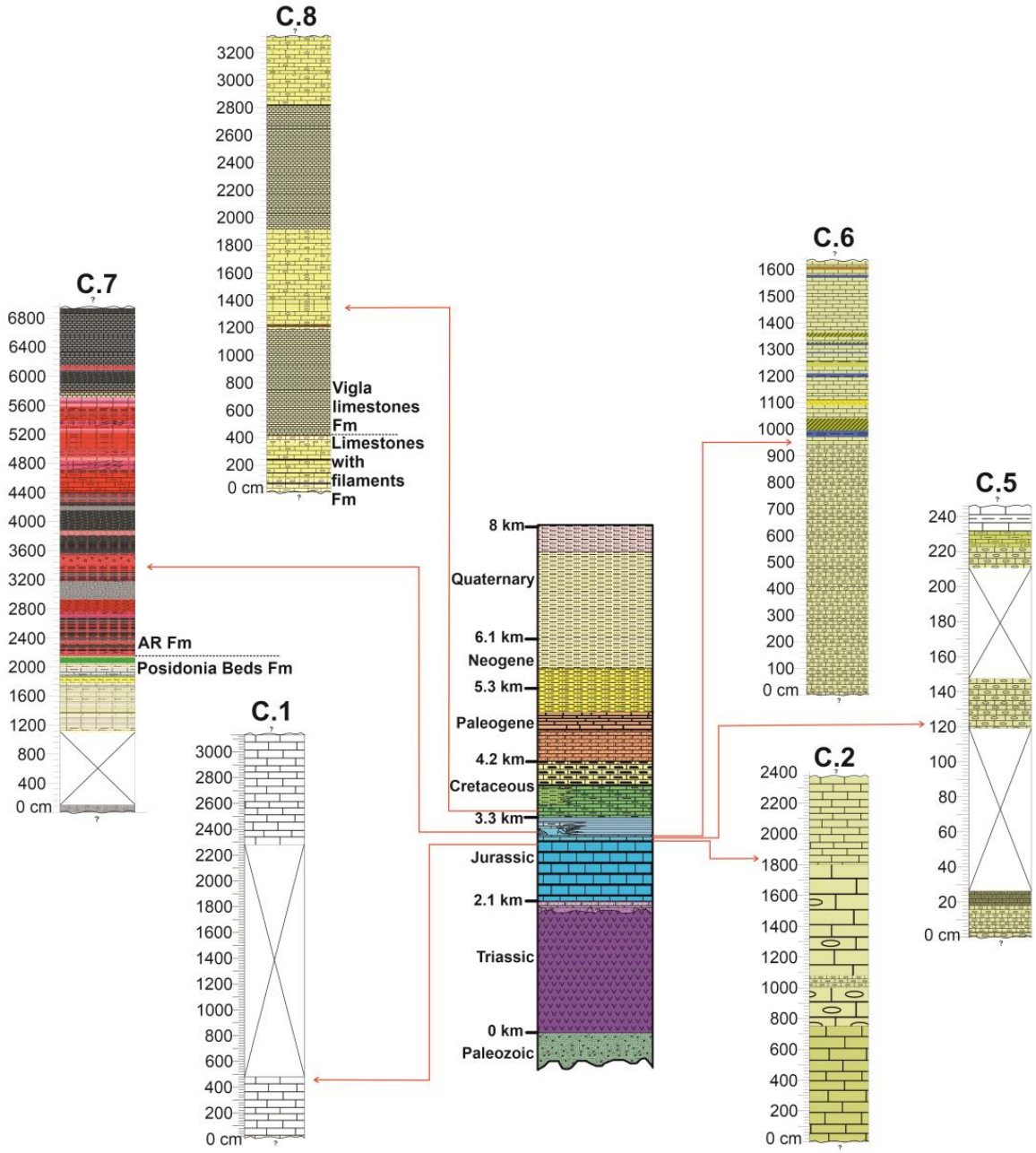

Figure 14. Correlations (red lines) of the stratigraphic columns of the sequences in this study with the synthetic stratigraphic column of the Ionian Basin. Lithology symbols can be seen above in the legends of the respective columns (Figures 2, 5, 6, 8, 10, 11 and 13).

4.5. Synsedimentary Deformation Structures Within the AR Fm

The lowest exposed part of the section consists of ~10 m of bedded limestone and calcareous shale, with variable dips, lateral thinning of units and local folding of limestone beds (1 in Figure 15a), and breakup of limestone beds into a shale matrix (2 in Figure 15a). The succession has an overall greenish-grey colour, quite distinct from the overlying red and white AR Fm. The base of the unit is not exposed, whereas at beach level, the top is marked by a few centimetres of greenish deformed fissile shale, conformably overlain by AR-type limestone (Figures 15b and 16c). Along the strike, in the cliff face, the contact appears rather irregular. As the internal details of this unit are not well exposed, it is simply termed the Lower Unit. It is probably either a complex slide or a debris-flow deposit with rafted blocks of bedded limestone, but we cannot exclude the possibility that the unit is in situ and suffered some internal deformation from the overlying slide.

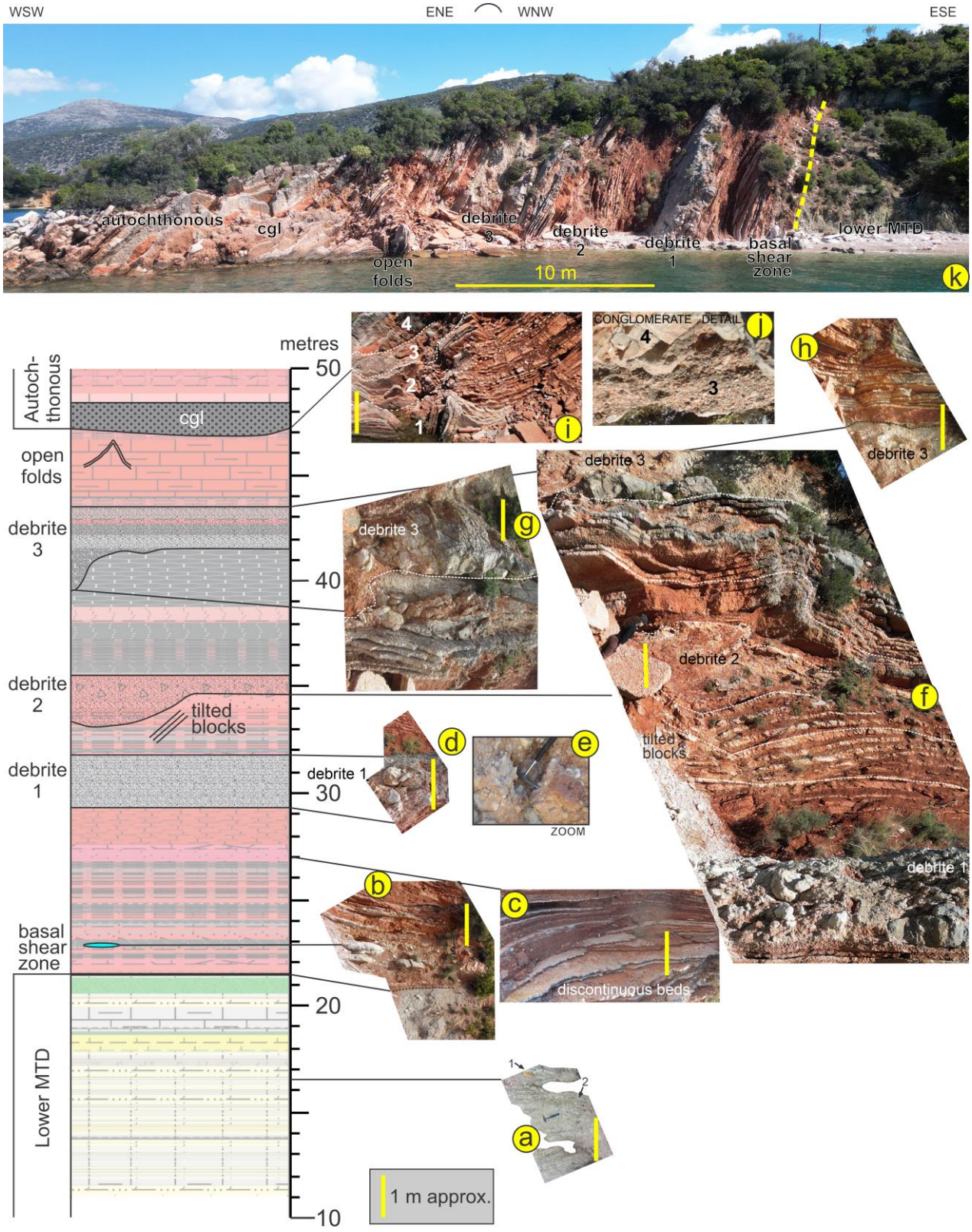

Figure 15. Stratigraphic column of the deformed interval in the AR Fm. (**a**–**j**) Field photographs illustrating detail in parts of the stratigraphic column. For further explanation, see text. Images are rotated and resized, so that layers interpreted as originally horizontal within the slide are horizontal and at approximately the same scale. Numbers in photos (**i**) and (**j**) refer to units discussed in text and further illustrated in Figure 17. (**k**) Drone image of the entire section.

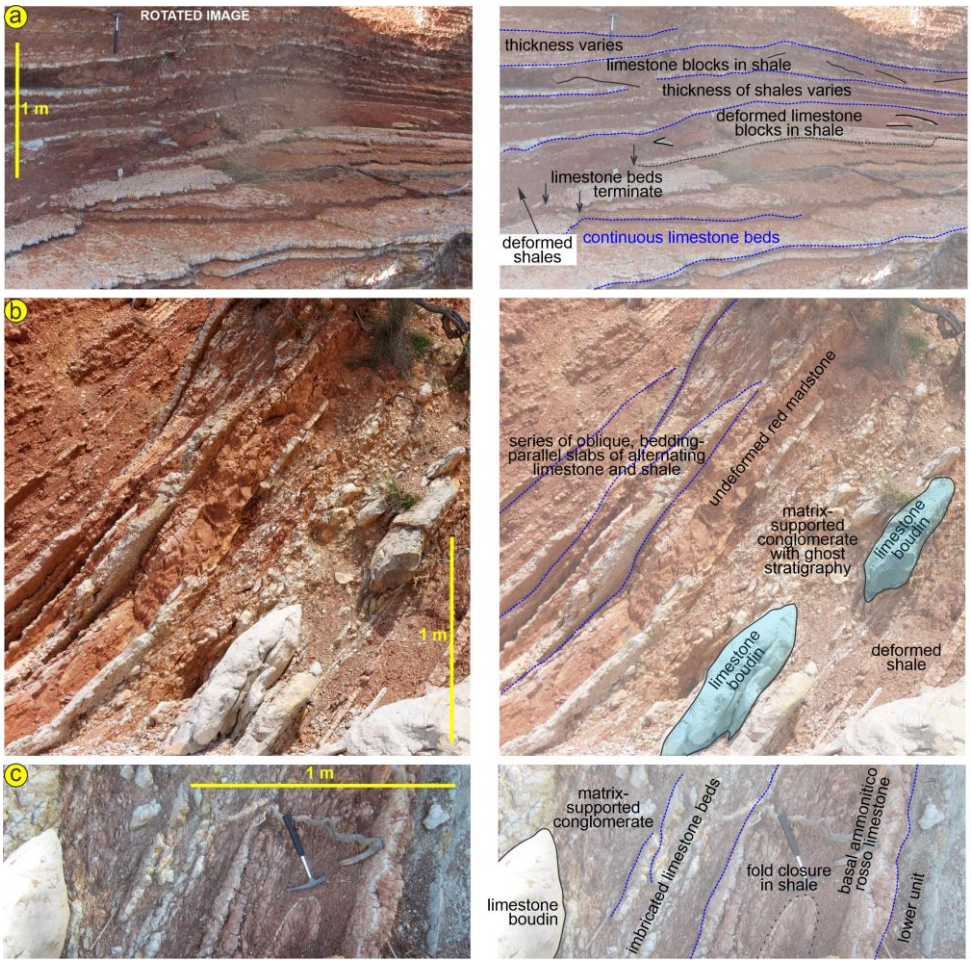

Figure 16. Field photographs of the base of the main slide interval below debrite 1. (**a**) Detail of Figure 15c showing deformation of limestone and shales. (**b**) Detail of Figure 15b showing large limestone boudins and overlying series of oblique, bedding-parallel slabs of alternating limestone and shale. (**c**) Detail of Figure 15b showing large limestone boudins and an underlying recumbent fold in shale above the contact with the Lower Unit.

The base of the AR Fm shows considerable synsedimentary deformation. The lowest shale unit has a recumbent fold closure (Figure 16c). It is overlain by discontinuous decimetre-scale boudins of micritic limestone enclosed in rubbly AR limestones and shale, with a ghost stratigraphy about 1 m thick (Figure 16b,c). This is overlain by 30 cm of apparently undeformed reddish marl and several metres of alternating nodular limestones and reddish shales with discontinuities between packets of limestone beds, thus creating a series of oblique, bedding-parallel slabs of alternating limestone and shale (Figure 15b). In places, limestone beds terminate or are boudinaged, and shales are deformed (Figure 15a). The proportion of limestone increases upward. This limestone is overlain by a 2 m thick, polymictic limestone, matrix-supported conglomerate interpreted as a debris-flow deposit, termed debrite 1 (Figure 15d–f).

Debrite 1 is overlain by about 1 m of reddish shales with discontinuous thin limestone beds, showing considerable fissility and deformation. Blocks of limestone show slickensides, suggesting sub-horizontal bedding plane slip on a later tectonic fault. Overlying bedded limestones show brittle deformation into metre-scale tilted blocks (Figure 15f), apparently as part of the slide mass, but with no evidence for the type of ductile boudins seen at the bottom of the AR section. Interbedded with the AR limestones is at least one graded calcirudite to calcarenite turbidite. The calcirudite is well sorted with rounded clasts up to 8 mm in size. Debrite 2 overlies the tilted blocks and is about 1 m thick (Figure 15f). It

is redder in colour than debrites 1 and 3 and is also matrix-supported. The upper surface of debrite 2 is folded into an open fold along with the immediately overlying 2 m of bedded limestone (Figure 15f). The degree of folding of the limestone beds decreases upwards, and the base of debrite 3 is irregular (Figure 15g). Debrite 3 is poorly sorted, with large subangular blocks, supported by a matrix of sand-sized limestone clasts and red mud (Figure 15f–h).

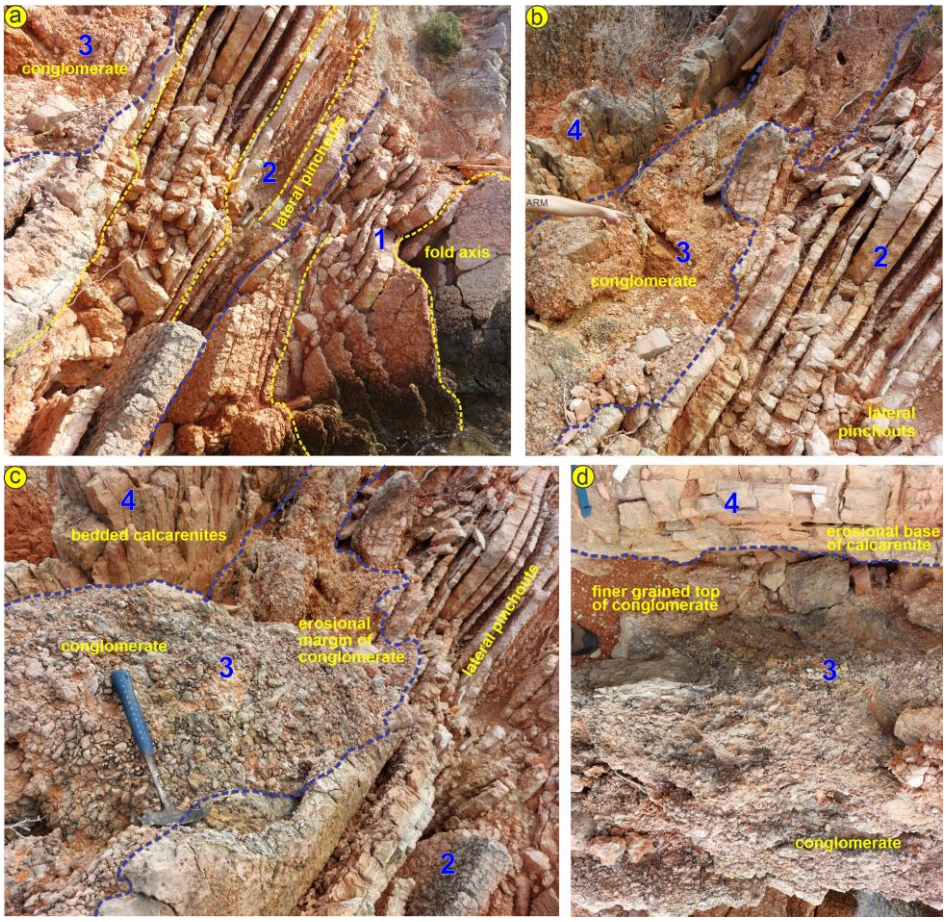

Figure 17. Field photographs of the setting of the conglomerate at the top of the main slide interval. Four units are recognized, separated by blue dashed lines: (1) Folded limestones in the main slide. (2) Overlying limestones and interbedded shale with lateral variability, suggesting that they are part of the main slide. (3) Conglomerate with an erosional base. (4) Overlying bedded calcarenites. (**a**) shows the relationship of the base of the conglomerate and unit (2) to the underlying folded limestone. (**b**) shows lateral pinchouts in unit (2) and the erosional base of the conglomerate. (**c**) shows the internal character of the conglomerate and its erosional base. (**d**) shows the entire thickness of the conglomerate, with the finer-grained top and the erosional base of the overlying calcarenite turbidites.

The top of debrite 3 is sharp and overlain by 30 cm of seemingly undeformed red shale and then an AR limestone section (Figure 15h) that in its upper part is deformed into a large open fold (1 in Figures 15i and 17a). The fold is unconformably overlain by about 1 m of bedded limestones with rapid lateral thinning (2 in Figures 15i and 17a–c), suggesting that it is also a block within the overall slide. These bedded limestones are overlain by a 1 m bed of sorted conglomerate (3 in Figures 15i,j and 17) with an erosional contact with the underlying limestones (Figure 17b,c). The conglomerate consists of rounded limestone pebbles (Figure 17c), with the upper part of the bed comprising fine pebbles and granules

(Figure 17d). Above this conglomerate is a succession of bedded red-grey calcarenites (4 in Figures 15i,j and 17).

Few clear directional structures are available. The torpedo-shaped boudins at the base of the slide (Figure 15b) are oriented approximately 205°. The fold near the top of the slide has an axis striking 130° and is asymmetric to the south (Figure 15i). Slickensides in blocks above debrite 2, which are probably a later tectonic fabric, plunge to ~300°. Taken together, these data suggest that slide movement was to the SW or SSW.

4.6. XRD Analysis

The XRD diffractograms of the studied limestone (from the AR Fm) samples revealed characteristic calcite peaks, as identified by their distinctive reflections. Additionally, the samples showed an additional peak that indicated the presence of quartz. Interestingly, in sample AR.6, one more peak was found that corresponds to the presence of glauconite. Among the five studied samples, there were no significant differences in the diffractogram peaks (Figure 18).

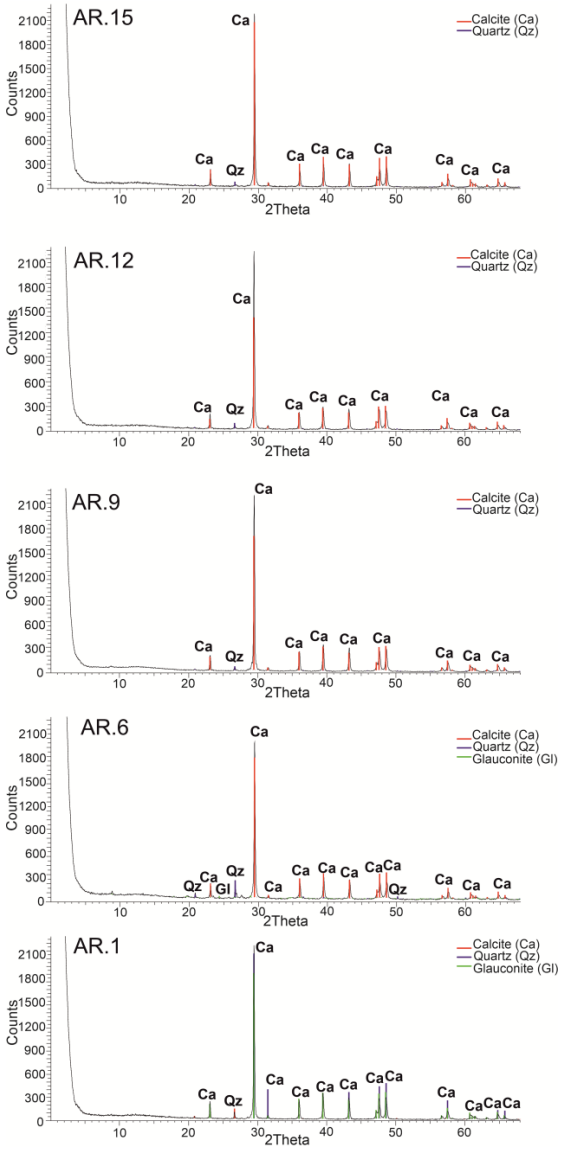

Figure 18. XRD diffractograms of the studied samples (AR.1, AR.9, AR.9, AR.12, AR.15).

5. Discussion

5.1. Depositional Environment of the Ammonitico Rosso Formation

The theories regarding the depositional environment of the AR Fm are still a subject of controversy today. Bernoulli et al. [25] considered the AR to have been formed in a littoral to shallow depositional environment, whereas other studies propose that the AR was deposited in the deeper parts of half-grabens ([24,45–47]). According to [2], the depth range of the AR Fm can be considered similar to the deeper parts of the epicontinental shelves. Microfacies analysis of Toarcian red nodular limestones (possibly the equivalent of the AR Fm) in Montenegro suggests that they were deposited in a low-energy, relatively deep-water environment (open-shelf environment) [48]. This study seems to agree with our findings on the AR Fm in Astakos. Both microfacies analysis (SMF-3 types corresponding to FZ 3, indicative of deposition in a deep-sea environment) and micropalaeontological analysis (identifying microfossils that lived in an open-shelf environment) [42] of the AR deposits in Astakos indicate that the deposition took place in a deep-water–open-shelf environment.

5.2. Interpretation of the Submarine Slide

The 20 m thick submarine slide deposits (Figure 15) include variably deformed blocks of AR Fm limestones and shales interbedded with matrix-supported conglomerates interpreted as debris-flow deposits. The basal 6 m shows predominant bedding-parallel deformation, including large torpedo-shaped boudins of micritic limestone (Figure 15). The upper part of the deposits above debrite 2 shows less evidence of strong vertical confining stress, with more open folds that deform both the bedded limestone and debrite 3 (Figure 15f,i). Many submarine slides consist of a thin debrite above the deformed blocks (e.g., [49]). The slide deposit is interpreted to comprise four imbricate slices, each some 5 m thick, which formed as toe thrusts in a single complex slide (Figure 19). All but the top slice are capped by a debrite. The alternative hypothesis that there were four discrete slides is rejected for several reasons: (1) It does not account for the restriction of strong bedding-parallel deformation, including boudinage, to the base of the lowest slice. (2) It does not account for the late folding of debrite 2 with its encasing limestones. (3) There is a lack of evidence of hard grounds or other seabed hiatuses to be expected at the irregular top of a submarine slide.

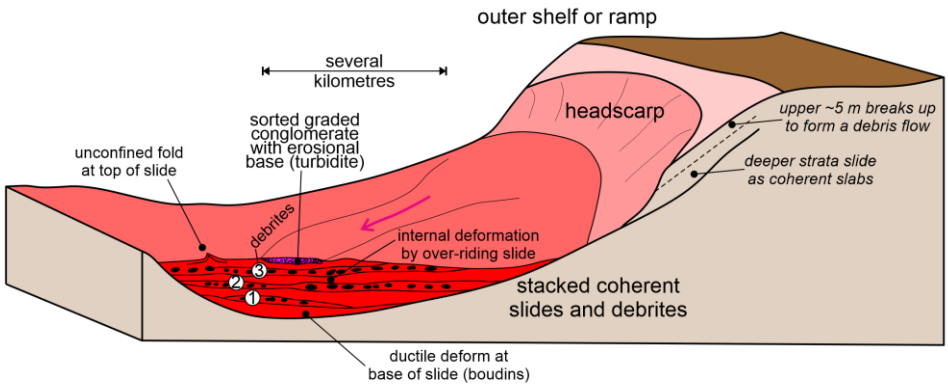

Figure 19. Model, not to scale, describing the mechanism of the formation of the AR slide.

The sorting and upward-fining grain size of the conglomerate that overlies the slide complex suggest that it is a single turbidite. Retrogressive failure of surficial material during the main slide event or by reactivation of the headwall following the slide can create a turbidity current [50], which, in the case here, would have largely bypassed the slide deposit. The limestone clasts resemble the nodular concretionary facies of the AR

and may have been reworked from the debrites or partially lithified AR limestones at the seabed. The erosional margin of the conglomerate (Figure 17b,c) demonstrates the erosional capacity of the turbidity current.

The beds that conformably overlie the conglomerate are grey calcarenites, at least in part turbidites, and lithologically distinct from the reddish nodular AR facies within the slide. They are assigned to the limestone with filaments Fm. The greenish-grey Lower Unit is correlated with the Lower Posidonia Fm. Thus, the AR Fm is present only as allochthonous blocks and debrites, deposited in deeper water than where the AR Fm was actually accumulated. The allochthonous nature of the AR Fm is recognized only because of the excellent outcrops in the high coastal cliffs. In the nearby intermittent road section, at PA.26 (Figure 1), the outcrop is too discontinuous to demonstrate an allochthonous origin.

A comparison can be made with other submarine landslide deposits in the literature. The most well known outcrops of slides are in sandstones and shales. These present similar larger-scale structures to the AR Fm slide, such as imbricate blocks of bedded sediment and repetitive stratigraphy in thrusts near the toe of the slide [8,51,52]. Flat-lying folds [53] and boudinages [54] are developed in shear zones, somewhat similar to the base of the AR slide (Figure 16b,c). In the classification of Sobiesiak et al. [55], the AR slide has a strong basal drag with shear deformation concentrated in the basal few metres of the slide. At a larger scale, such slides show basal erosion by dragging tools into the substrate [55]; in the case of our study, the lower contact high in the cliff appears irregular, but the details cannot be resolved. It is possible that some deformation is propagated deeper into the substrate (as in the discontinuous no-slip basal deformation of [55]), but exposure in the Lower Unit is insufficient to demonstrate this. Microfossils in the Lower Unit are similar to those in the AR, suggesting that the Lower Unit is also allochthonous.

Many of the distinctive small-scale features of sandstone–shale slides are absent in our carbonate slide. Strain is not concentrated in the finer-grained marls in the same way as it affects shales. Our boudins in micrite show much greater internal strain than typical sandstone boudins in which the original stratification is commonly preserved [55]. Slides developed in limestone successions are reported to consist principally of variably deformed slabs of bedded limestone [56] and commonly thick debrite horizons [57–59], as in our AR example. These differences between siliciclastic and carbonate submarine landslides largely result from the early partial lithification of limestones near the seafloor and the resulting decrease in porosity. Such lithification is represented in the AR Fm by the nodular limestones that are the source of clasts in the overlying turbidite conglomerate.

Cenozoic deformation and the lack of Lower Jurassic outcrops make it difficult to assess the palaeogeographic setting of the studied AR Fm. The half-graben basins of the Ionian Basin may well have been on a scale similar to the Southern California Borderland, with basin floors at 700–1500 m water depth. Smaller submarine landslides there have runout distances of 5–10 km and are interpreted to have been triggered by earthquakes [60]. Quaternary glacio-eustatic sea level changes and high clastic input mean that the Borderland is not an analogue for sedimentation processes on the outer parts of the continental shelves. Rather, well-studied peri-Tethyan Lower Jurassic carbonate ramps e.g., [61] are better morphological analogues for the depositional setting of the autochthonous AR Fm. A transport distance of 10 km would be sufficient for a turbidity current to develop from a watery debris flow formed by headwall collapse [50].

5.3. Mass-Transport Events in the AR Fm During the Early Jurassic

Many researchers have reported the presence of mass-transport deposits ("slumps" in the older literature) within the AR Fm during the Pliensbachian–Toarcian, although most were not analyzed in detail. Bernoulli and Renz [25] described intercalations of slump conglomerates and calc-turbidites composed of redeposited carbonates from a platform (broken shells, ooids, oncoids) and intraclasts of neritic limestones. They considered that these turbidites were formed due to the presence of slopes along the margins of a carbonate platform, implying that the basin deposits were deposited in relatively deep waters (at least several hundred metres or more). Also, Karakitsios [17] referred to the existence of slumps within the syn-rift succession of the Ionian Basin, but without proceeding to any further analysis. The author of [62] studied the Jurassic redeposited pelagic sediments in the Central Mediterranean area (Western Greece, Marche-Umbria, and Lombardian Alps (Central and Northern Italy, respectively)) and pointed out that in the Toarcian, the AR Fm of Western Greece consisted of intercalations of graded conglomerates, where the pebbles derived from limestones of the Sinies Fm. The pebbles in our study area originated from the AR Fm. Debris flows within Toarcian black shales (just below the limestones with filaments Fm), as well as turbidites, breccias, and olistostromes within the AR Fm, have also been found close to Igoumenitsa (Northwestern Greece) [63]. All these observations suggest that, regionally, the most active syn-rift subsidence took place in the Toarcian. In other rift basins, this phase is marked by maximum steepening of the basin margins and the greatest evidence for in situ synsedimentary deformation and landsliding, generally 10–15 Ma after the onset of rifting [64,65]. In the Ionian Basin, rifting is dated from the base of the Pliensbachian [24], with rapid Toarcian subsidence 10–15 Ma later.

5.4. Lower Posidonia Bed and AR Fms

Based on [66], there are two coeval facies that developed within the Ionian Basin during the Toarcian: (i) organic-rich black shales (Lower Posidonia beds) that were deposited in basins, and (ii) pelagic red nodular limestones (AR Fm) that were deposited on palaeotopographic highs or seamounts. These two facies, however, can occur within the same outcrop, such as in Kouklessi (Western Greece), as noted by [25], and also in our study area (Figure 15). However, in our study area, the Lower Posidonia Fm beds are not black in colour, and they are also not organic-rich. Also, according to [29], the sedimentation rate of the AR Fm in the study area is 0.0083 mm/yr for the lower part, and a little higher for the upper part (0.0085 mm/yr). These rates are almost three times higher than the average rate of sedimentation reported by [1] for the AR Fm. Therefore, the previously reported rate [29] probably did not take into account the duplication of sections in the complex slide (Figure 19).

Moreover, after the geological mapping and microfacies analysis of the study area, the pre-existing geological map was corrected (Figure 20). The Sinies Fm limestones were separated from those of the Pantokrator Fm. In the central part of the map, Vigla Fm limestones have been recognized. The new map indicates the dip and dip directions of the beds, as well as some new recorded faults.

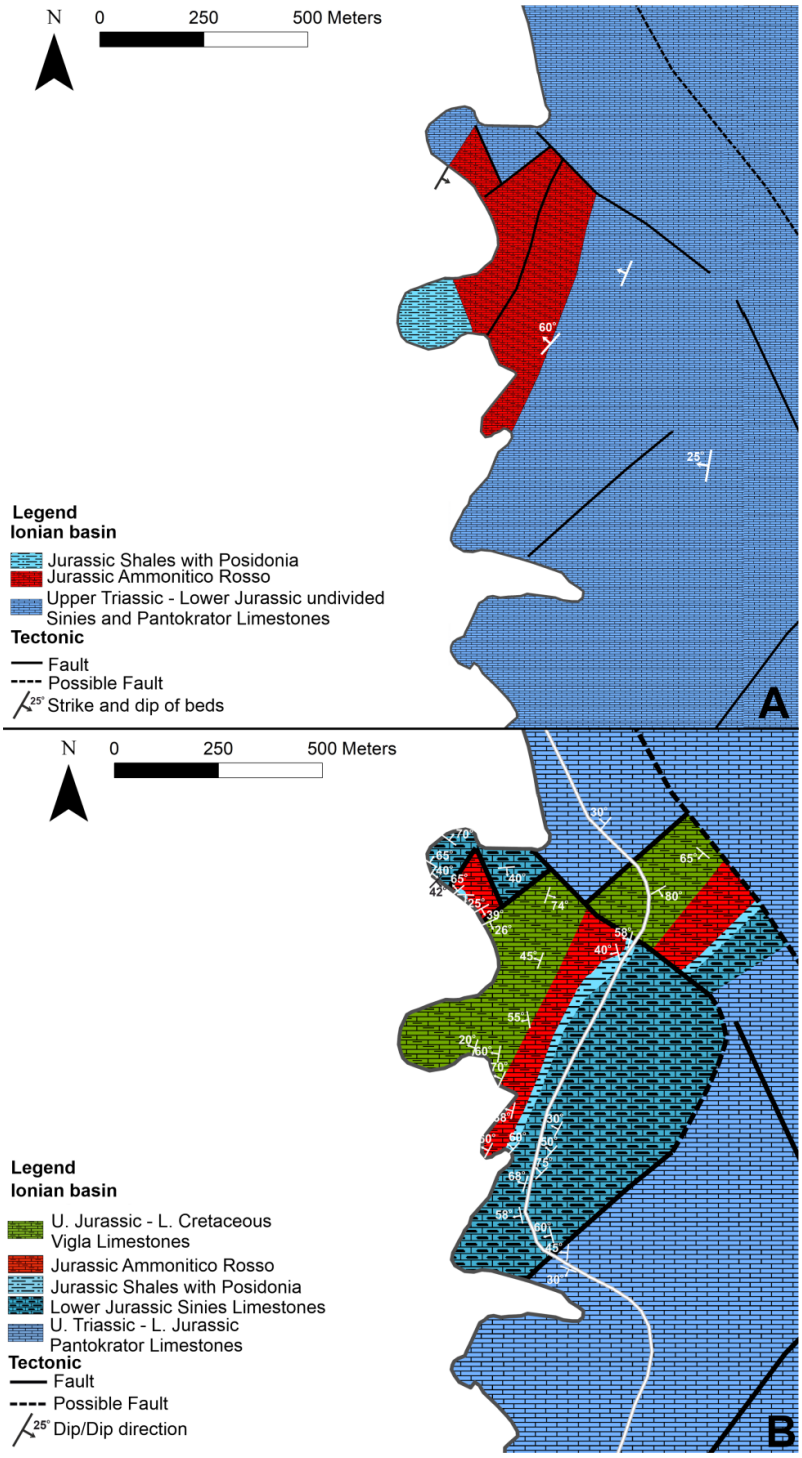

Figure 20. The digitized pre-existing geological map [67] of the study area (**A**) and the new geological map after this study (**B**).

5.5. Lithotypes of AR Fm

Cecca et al. [3] defined two different lithotypes for the AR Fm: a marly and a calcareous lithotype. The marly lithotype, which was last developed in the Toarcian, is thicker than the calcareous lithotype. In the study area, the AR Fm is of the marly lithotype. According to [3], the marly lithotype developed in slope areas (tilted blocks) extending into basinal environments, leading to the presence of gravity deposits such as slumps and debris flows. On the other hand, calcareous lithotypes were not frequent in the Toarcian and developed on swells (pelagic ridges, deep submarine horsts, tilted blocks,

etc.). This lithotype is characterized by the presence of hard grounds with encrusted Fe-Mn nodules and stromatolitic overgrowths. The Toarcian AR Fm, mainly of the marly lithotype, developed between 15° and 30° N latitude and is widespread in the Mediterranean part of the Tethys Ocean, on the Apulian promontory and the North African margin (the passive margin of Northern Gondwana), and at the northern margin of the Tethys Ocean on the southern Iberian margin.

5.6. Basin Evolution

In the Ionian Basin, inversion tectonic structures occur [68]. During the Early Jurassic, the Ionian Basin began to open due to extensional stress that affected the Tethys Ocean [17,25,68]. This extensional stress initiated the formation of a rift basin, leading to deeper-water sedimentation (Stage 1 in Figure 21). This extension created accommodation for the deposition of the Sinies limestone Fm, Posidonia bed Fm, AR Fm, limestones with filaments Fm, Vigla limestone Fm, and all the other formations in the Ionian Basin until the Paleogene (syn-rift successions).

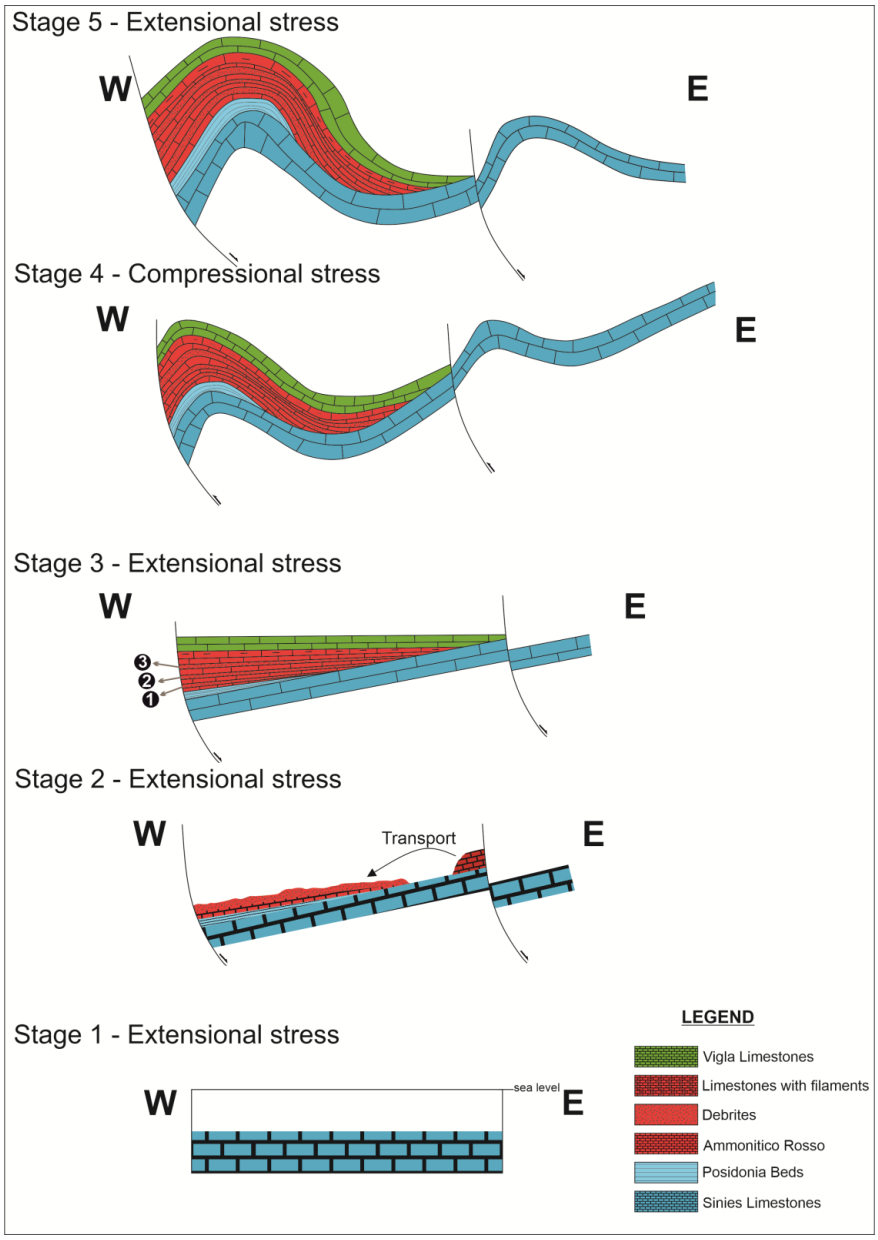

Figure 21. Basin evolution model of the study area from the Early Jurassic to the present.

From the Middle Eocene to the Middle Miocene, the tectonic regime changed from extensional to compressional stress (Stage 4 in Figure 21). However, from the Middle Miocene to the present, the stress has become extensional once again [68].

During the Early to Middle Jurassic extensional phase, slopes were formed in the Ionian Basin, leading to submarine landsliding events, such as the ones that have also been observed in the study area.

6. Conclusions

In the frame of this study, eight sedimentary sequences in the Astakos area (Greece) have been studied. Detailed sedimentological, tectonic, and biostratigraphic analyses of both carbonate and clastic sediments have been conducted. They belong to the Pantokrator, Sinies, AR, and Vigla Fms of the Ionian Zone. A new version of the geological map of the area is presented herein. Moreover, the following findings have been reported:

- Biostratigraphic analyses showed that the studied sedimentary sequences bear an age of Lower Jurassic–Lowermost Cretaceous. Moreover, there are indications that some *Globuligerina* tests occurred earlier than previously known; their first appearance probably occurred during the Pliensbachian.
- The palaeoenvironmental reconstruction of the studied sequence revealed two distinct depositional environments: deep-water to open-shelf settings and platform-margin reefs.
- Deposition of the AR Fm in Astakos took place in a deep-water environment, and more specifically in an open-shelf environment. The studied sedimentary sequence, though, comprises an allochthonous submarine slide deposit, consisting of four imbricate slices capped by debrites (except the upper one) rather than four discrete slides. Upwards, a conglomerate with reworked limestone clasts has been deposited as a result of a single turbidite. The sequence closes with sediments of the limestone with filaments and Lower Posidonia bed Fms.
- The autochthonous AR Fm depositional setting fits well with a carbonate ramp, on which turbidity currents with a transport distance of several kilometres would be developed from a watery debris flow formed by headwall collapse.
- The discovery of the AR Fm slide has a profound effect on the reported sedimentation rates for the area, which until now have not taken into consideration the duplication of the layers, and which thus must be significantly lower.
- The AR Fm slides show similarities with other larger-scale studied sandstone–shale slides (i.e., imbricate blocks of bedded sediment, repetitive stratigraphy, flat-lying folds, boudinages, etc.), but some characteristics are missing due to insufficient exposure. Moreover, many small-scale features of sandstone–shale slides do not exist in the AR Fm slides. This is attributed to the early partial lithification of limestones near the seafloor and the resulting decrease in porosity which is present in the studied sediments.
- The present study contributes to the Early Jurassic Ionian Basin Evolution by reporting a case where a submarine landsliding event happened due to the existence of slopes formed during the Early Jurassic extensional phase.

The AR Fm deposition across Greece has been a matter of debate since no detailed studies have been conducted until now. This work highlights the complexity and the importance of studying each individual section in detail. Further investigation of AR Fm outcrops of the Ionian Unit in the future will expand our knowledge of the depositional environment, the evolution, and the age of this formation across Greece.

Author Contributions: Conceptualization, G.I. and A.Z.; methodology, A.Z., G.I., D.J.W.P. and V.G.; software, V.G. and D.J.W.P.; formal analysis, G.I. and V.G.; investigation, V.G., D.J.W.P., G.P.-P., A.Z., P.P., A.Z. and G.I.; data curation, V.G.; writing—original draft preparation, V.G., D.J.W.P. and A.Z.; writing—review and editing, V.G., A.Z., D.J.W.P., G.P.-P., N.B., P.P. and G.I.; visualization, V.G. and G.I.; supervision, G.I.; project administration, G.I. All authors have read and agreed to the published version of the manuscript.

Funding: Vasilis Golfinopoulos, as a PhD student, was financially supported by the "Andreas Mentzelopoulos Scholarships for the preparation of doctoral dissertation at the University of Patras", project No. 33720000.

Data Availability Statement: All data supporting the findings of this study are included within the article. No additional data were created or analyzed during the study.

Acknowledgments: We would like to express our sincere gratitude to Lampropoulou Paraskevi of the Department of Geology at the University of Patras for conducting the XRD analysis. We also extend our warm thanks to Vasilios Giamas for his valuable assistance with interpreting the XRD results. Special thanks go to the members of the Palaeontology and Stratigraphy Laboratory at the University of Patras, including Marianthi Tzortzi, Irena Pappa, and Maria Groumpou, for their essential support during the fieldwork.

Conflicts of Interest: The authors declare no conflicts of interest. The funders had no role in the design of the study; in the collection, analyses, or interpretation of data; in the writing of the manuscript; or in the decision to publish the results.

References

1. Jenkyns, H.C. Origin of Red Nodular Limestones (Ammonitico Rosso, Knollenkalke) in the Mediterranean Jurassic: A Diagenetic Model. In *Pelagic Sediments: On Land and Under the Sea*; Wiley-Blackwell: Hoboken, NJ, USA, 1975; pp. 249–271.
2. Oloriz, F.; Caracuel, J.E.; Ruiz Heras, J.J. Numerical Analysis of Sedimentary Components; a Key for Interpretation of Macroscopic and Microscopic Features in Ammonitico Rosso Facies (Uppermost Jurassic-Lowermost Cretaceous). *J. Sediment. Res.* **1995**, *65*, 234–243.
3. Cecca, F.; Fourcade, E.; Azéma, J. The Disappearance of the "Ammonitico Rosso". *Palaeogeogr. Palaeoclimatol. Palaeoecol.* **1992**, *99*, 55–70. [CrossRef]
4. Müller, J.; Fabricius, F. Magnesian-calcite Nodules in the Ionian Deep Sea: An Actualistic Model for the Formation of Some Nodular Limestones. In *Pelagic Sediments: On Land and Under the Sea*; Wiley-Blackwell: Hoboken, NJ, USA, 1975; pp. 235–247.
5. Rettger, R.E. Experiments on Soft-Rock Deformation. *Am. Assoc. Pet. Geol. Bull.* **1935**, *19*, 271–292.
6. Ferrill, D.A.; Smart, K.J.; Lehrmann, D.J.; Morris, A.P.; McGinnis, R.N. Synsedimentary Slump Folding: Examples and Consequences of an under-Recognized Process in Epicratonic Basins. *Mar. Pet. Geol.* **2023**, *152*, 106274. [CrossRef]
7. García-Tortosa, F.J.; Alfaro, P.; Gibert, L.; Scott, G. Seismically Induced Slump on an Extremely Gentle Slope (<1°) of the Pleistocene Tecopa Paleolake (California). *Geology* **2011**, *39*, 1055–1058. [CrossRef]
8. Alsop, G.I.; Marco, S.; Levi, T.; Weinberger, R. Fold and Thrust Systems in Mass Transport Deposits. *J. Struct. Geol.* **2017**, *94*, 98–115. [CrossRef]
9. Welbon, A.I.F.; Brockbank, P.J.; Brunsden, D.; Olsen, T.S. Characterizing and Producing from Reservoirs in Landslides: Challenges and Opportunities. *Geol. Soc. Lond. Spec. Publ.* **2007**, *292*, 49–74. [CrossRef]
10. Novak, A.; Egenhoff, S. Soft-Sediment Deformation Structures as a Tool to Recognize Synsedimentary Tectonic Activity in the Middle Member of the Bakken Formation, Williston Basin, North Dakota. *Mar. Pet. Geol.* **2019**, *105*, 124–140. [CrossRef]
11. Bourli, N.; Maravelis, A.G.; Zelilidis, A. Classification of Soft-Sediment Deformation in Carbonates Based on the Lower Cretaceous Vigla Formation, Kastos, Greece. *Int. J. Earth Sci.* **2020**, *109*, 2599–2614. [CrossRef]
12. Bourli, N.; Iliopoulos, G.; Zelilidis, A. Reassessing Depositional Conditions of the Pre-Apulian Zone Based on Synsedimentary Deformation Structures during Upper Paleocene to Lower Miocene Carbonate Sedimentation, from Paxoi and Anti-Paxoi Islands, Northwestern End of Greece. *Minerals* **2022**, *12*, 201. [CrossRef]
13. Dimopoulos, N.; Zoumpouli, E.; Bourli, N.; Papadopoulou, P.; Iliopoulos, G.; Zelilidis, A. A Giant Slide within the Upper Cretaceous Limestones as an Indicator for Fault Activity Dating and Basin Evolution. In Proceedings of the 4th International Electronic Conference on Geosciences (IECG) 2022, Online, 1–15 December 2022; MDPI: Basel, Switzerland, 2023; p. 8.
14. Alvarez, W.; Lowrie, W. Magnetic Stratigraphy Applied to Synsedimentary Slumps, Turbidites, and Basin Analysis: The Scaglia Limestone at Furlo (Italy). *Geol. Soc. Am. Bull.* **1984**, *95*, 324. [CrossRef]

15. Bourli, N.; Pantopoulos, G.; Maravelis, A.G.; Zoumpoulis, E.; Iliopoulos, G.; Pomoni-Papaioannou, F.; Kostopoulou, S.; Zelilidis, A. Late Cretaceous to Early Eocene Geological History of the Eastern Ionian Basin, Southwestern Greece: A Sedimentological Approach. *Cretac. Res.* **2019**, *98*, 47–71. [CrossRef]
16. Moforis, L.; Kontakiotis, G.; Janjuhah, H.T.; Zambetakis-Lekkas, A.; Galanakis, D.; Paschos, P.; Kanellopoulos, C.; Sboras, S.; Besiou, E.; Karakitsios, V.; et al. Sedimentary and Diagenetic Controls across the Cretaceous—Paleogene Transition: New Paleoenvironmental Insights of the External Ionian Zone from the Pelagic Carbonates of the Gardiki Section (Epirus, Western Greece). *J. Mar. Sci. Eng.* **2022**, *10*, 1948. [CrossRef]
17. Karakitsios, V. The Influence of Preexisting Structure and Halokinesis on Organic Matter Preservation and Thrust System Evolution in the Ionian Basin, Northwest Greece. *Am. Assoc. Pet. Geol. Bull.* **1995**, *79*, 960–980. [CrossRef]
18. Papanikolaou, D.I. *The Geology of Greece*; Springer Nature: Berlin/Heidelberg, Germany, 2021; ISBN 3030607313.
19. Karakitsios, V.; Kvaček, Z.; Mantzouka, D. The First Plant Megafossil in the Early Jurassic of Greece: Brachyphyllum (Coniferales) from the Lower Posidonia Beds (Toarcian) in the Ionian Zone (NW Greece) and Its Palaeogeographic Implications. *Neues Jahrb. Für Geol. Und Paläontologie Abh.* **2015**, *278*, 79–94. [CrossRef]
20. Kontakiotis, G.; Moforis, L.; Karakitsios, V.; Antonarakou, A. Sedimentary Facies Analysis, Reservoir Characteristics and Paleogeography Significance of the Early Jurassic to Eocene Carbonates in Epirus (Ionian Zone, Western Greece). *J. Mar. Sci. Eng.* **2020**, *8*, 706. [CrossRef]
21. Zelilidis, A.; Piper, D.J.W.; Vakalas, I.; Avramidis, P.; Getsos, K. Oil and Gas Plays in Albania: Do Equivalent Plays Exist in Greece? *J. Pet. Geol.* **2003**, *26*, 29–48. [CrossRef]
22. Zelilidis, A.; Maravelis, A.G.; Tserolas, P.; Konstantopoulos, P.A. An Overview of the Petroleum Systems in the Ionian Zone, Onshore NW Greece and Albania. *J. Pet. Geol.* **2015**, *38*, 331–348. [CrossRef]
23. Danelian, T.; De Wever, P.; Azéma, J. Palaeoceanographic Significance of New and Revised Palaeontological Datings for the Onset of Vigla Limestone Sedimentation in the Ionian Zone of Greece. *Geol. Mag.* **1997**, *134*, 869–872. [CrossRef]
24. Karakitsios, V. Western Greece and Ionian Sea Petroleum Systems. *Am. Assoc. Pet. Geol. Bull.* **2013**, *97*, 1567–1595. [CrossRef]
25. Bernoulli, D.; Renz, O. Jurassic Carbonate Facies and New Ammonite Faunas from Western Greece. *Eclogae Geol. Helv.* **1970**, *63*, 573–607. [CrossRef]
26. British Petroleum Company. *The Geological Results of Petroleum Exploration in Western Greece*; Institute for Geology and Subsurface Research: Athens, Greece, 1971; Volume 10.
27. Clews, J.E. Mesozoic and Cenozoic Geodynamic Evolution of Western Greece. Ph.D. Thesis, University of Wales, Wales, UK, 1989.
28. Underhill, J.R. Late Cenozoic Deformation of the Hellenide Foreland, Western Greece. *Geol. Soc. Am. Bull.* **1989**, *101*, 613–634. [CrossRef]
29. Birch, W.G. Palaeomagnetic Studies in Western and Central Greece: Tectonic Evolution of the Aegean Domain since the Triassic. Ph.D. Thesis, University of Liverpool, Liverpool, UK, 1990.
30. Bourli, N.; Iliopoulos, G.; Papadopoulou, P.; Zelilidis, A. Microfacies and Depositional Conditions of Jurassic to Eocene Carbonates: Implication on Ionian Basin Evolution. *Geosciences* **2021**, *11*, 288. [CrossRef]
31. Bourli, N.; Kokkaliari, M.; Iliopoulos, I.; Pe-Piper, G.; Piper, D.J.W.; Maravelis, A.G.; Zelilidis, A. Mineralogy of Siliceous Concretions, Cretaceous of Ionian Zone, Western Greece: Implication for Diagenesis and Porosity. *Mar. Pet. Geol.* **2019**, *105*, 45–63. [CrossRef]
32. Avramidis, P.; Zelilidis, A. The Nature of Deep-Marine Sedimentation and Palaeocurrent Trends as Evidence of Pindos Foreland Basin Fill Conditions. *Episodes* **2001**, *24*, 252–256. [CrossRef]
33. Avramidis, P.; Zelilidis, A.; Vakalas, I.; Kontopoulos, N. Interactions Between Tectonic Activity And Eustatic Sea-Level Changes In The Pindos and Mesohellenic Basins, NW Greece: Basin Evolution And Hydrocarbon Potential. *J. Pet. Geol.* **2002**, *25*, 53–82. [CrossRef]
34. Golfinopoulos, V. Biostratigraphic Study, Microfacies Analyses and Hydrocarbon Prospectivity of the Jurassic—Cretaceous Shale Formations, North of Petousi Fault in Epirus. Master's Thesis, Aristotle University of Thessaloniki, Patras, Greece, 2022.
35. Folk, R.L. Practical Petrographic Classification of Limestones. *Am. Assoc. Pet. Geololists Bull.* **1959**, *43*, 1–38.
36. Folk, R.L.; Ham, W.E. *Classification of Carbonate Rocks*; American Association of Petroleum Geologists: Tulsa, OK, USA, 1962; pp. 62–84.
37. Dunham, R.J. Spectral Subdivision of Limestone Type. In *Classification of Carbonate Rocks*; American Association of Petroleum Geologists: Tulsa, OK, USA, 1962; Volume 1, pp. 62–84.
38. Flügel, E. *Microfacies of Carbonate Rocks*; Springer: Berlin/Heidelberg, Germany, 2004; ISBN 978-3-662-08728-2.
39. Wilson, J.L. *Carbonate Facies in Geologic History*; Springer: New York, NY, USA, 1975; ISBN 978-0-387-90343-9.
40. Flügel, E. *Microfacies of Carbonate Rocks*, 2nd ed.; Springer: Berlin/Heidelberg, Germany, 2010; ISBN 978-3-642-03795-5.
41. Gradstein, F.; Waskowska, A. New Insights into the Taxonomy and Evolution of Jurassic Planktonic Foraminifera. *Swiss J. Palaeontol.* **2021**, *140*, 1. [CrossRef]

42. Golfinopoulos, V.; Papadopoulou, P.; Zelilidis, A.; Iliopoulos, G. Palaeoenvironmental Interpretation of the Lower Jurassic Formations in the Ionian Basin: First Stereoscopic Record of Benthic Foraminifera and Ostracods Assemblages from Greece. 2024; *to be submitted*.
43. Benzaggagh, M. Discussion on the Calpionellid Biozones and Proposal of a Homogeneous Calpionellid Zonation for the Tethyan Realm. *Cretac. Res.* **2020**, *114*, 104184. [CrossRef]
44. Verga, D.; Premoli Silva, I. Early Cretaceous Planktonic Foraminifera from the Tethys: The Small, Few-Chambered Representatives of the Genus Globigerinelloides. *Cretac. Res.* **2003**, *24*, 305–334. [CrossRef]
45. Kafousia, N.; Karakitsios, V.; Mattioli, E.; Kenjo, S.; Jenkyns, H.C. The Toarcian Oceanic Anoxic Event in the Ionian Zone, Greece. *Palaeogeogr. Palaeoclimatol. Palaeoecol.* **2014**, *393*, 135–145. [CrossRef]
46. Karakitsios, V.; Chatzicharalampous, E. Biostratigraphy and Sedimentology of the Ionian Zone Ammonitico Rosso in the Mavron Oros Area (NW Epirus, Greece)-Paleogeographic Implications. *Bull. Geol. Soc. Greece* **2013**, *47*, 136–145. [CrossRef]
47. Rigakis, N.; Karakitsios, V. The Source Rock Horizons of the Ionian Basin (NW Greece). *Mar. Pet. Geol.* **1998**, *15*, 593–617. [CrossRef]
48. Djakovic, M.; Gawlick, H.-J.; Sudar, M. Early-Middle Jurassic Stepwise Deepening in the Transitional Facies Belt between the Adriatic Carbonte Platform Basement and Neo-Tethys Open Shelf in Northeastern Montenegro Evidenced by New Ammonoid Data from the Early Late Pliensbachian (Lavinianum Zone). *Geol. Anal. Balk. Poluostrva* **2021**, *82*, 1–25. [CrossRef]
49. Piper, D.J.W.; Pirmez, C.; Manley, P.L.; Long, D.; Flood, R.D.; Normark, W.R.; Showers, W. Mass-Transport Deposits of the Amazon Fan. In *Proceedings-Ocean Drilling Program Scientific Results*; National Science Foundation: Alexandria, VA, USA, 1997; pp. 109–146.
50. Piper, D.J.W.; Cochonat, P.; Morrison, M.L. The Sequence of Events around the Epicentre of the 1929 Grand Banks Earthquake: Initiation of Debris Flows and Turbidity Current Inferred from Sidescan Sonar. *Sedimentology* **1999**, *46*, 79–97. [CrossRef]
51. Sobiesiak, M.S.; Kneller, B.; Alsop, G.I.; Milana, J.P. Internal Deformation and Kinematic Indicators within a Tripartite Mass Transport Deposit, NW Argentina. *Sediment. Geol.* **2016**, *344*, 364–381. [CrossRef]
52. Sun, Q.; Xie, X.; Wu, S.; Yin, G. Thrust Faults Promoted Hydrocarbon Leakage at the Compressional Zone of Fine-Grained Mass-Transport Deposits. *Front. Earth Sci.* **2021**, *9*, 764319. [CrossRef]
53. de Lima Rodrigues, M.C.N.; Trzaskos, B.; Alsop, G.I.; Vesely, F.F. Making a Homogenite: An Outcrop Perspective into the Evolution of Deformation within Mass-Transport Deposits. *Mar. Pet. Geol.* **2020**, *112*, 104033. [CrossRef]
54. Sobiesiak, M.S.; Buso, V.V.; Kneller, B.; Alsop, G.I.; Milana, J.P. *Block Generation, Deformation, and Interaction of Mass-Transport Deposits with the Seafloor: An Outcrop-Based Study of the Carboniferous at Cerro Bola, NW Argentina*; American Geophysical Union: Washington, DC, USA, 2020; Volume 246, pp. 91–104.
55. Sobiesiak, M.S.; Kneller, B.; Alsop, G.I.; Milana, J.P. Styles of Basal Interaction beneath Mass Transport Deposits. *Mar. Pet. Geol.* **2018**, *98*, 629–639. [CrossRef]
56. Spalluto, L.; Moretti, M.; Festa, V.; Tropeano, M. Seismically-Induced Slumps in Lower-Maastrichtian Peritidal Carbonates of the Apulian Platform (Southern Italy). *Sediment. Geol.* **2007**, *196*, 81–98. [CrossRef]
57. Bao, Z. Continental Slope Limestones of Lower and Middle Triassic, South China. *Sediment. Geol.* **1998**, *118*, 77–93. [CrossRef]
58. Jablonska, D.; Di Celma, C.; Korneva, I.; Tondi, E.; Alsop, I. Mass-Transport Deposits within Basinal Carbonates from Southern Italy. *Ital. J. Geosci.* **2016**, *135*, 30–40. [CrossRef]
59. Jablonská, D.; Di Celma, C.N.; Alsop, G.I.; Tondi, E. Internal Architecture of Mass-transport Deposits in Basinal Carbonates: A Case Study from Southern Italy. *Sedimentology* **2018**, *65*, 1246–1276. [CrossRef]
60. Walton, M.A.L.; Conrad, J.E.; Papesh, A.G.; Brothers, D.S.; Kluesner, J.W.; McGann, M.; Dartnell, P. A Comprehensive Assessment of Submarine Landslides and Mass Wasting Processes Offshore Southern California. *Geochem. Geophys. Geosyst.* **2024**, *25*, e2023GC011258. [CrossRef]
61. Pierre, A.; Durlet, C.; Razin, P.; Chellai, E.H. Spatial and Temporal Distribution of Ooids along a Jurassic Carbonate Ramp: Amellago Outcrop Transect, High-Atlas, Morocco. *Geol. Soc. Lond. Spec. Publ.* **2010**, *329*, 65–88. [CrossRef]
62. Bernoulli, D. Redeposited Pelagic Sediments in the Jurassic of the Central Mediterranean Area. In *Annales Instituti Geologici Publici Hungarici*; Hungarian Geological Institute: Budapest, Hungary, 1971; Volume 54, pp. 71–90.
63. Walzebuck, J.P. Bedding Types of the Toarcian Black Shales in NW-Greece. In *Cyclic and Event Stratification*; Springer: Berlin/Heidelberg, Germany, 1982; pp. 512–525.
64. Lambiase, J.J.; Bosworth, W. Structural Controls on Sedimentation in Continental Rifts. *Geol. Soc. Lond. Spec. Publ.* **1995**, *80*, 117–144. [CrossRef]
65. Tang, W.; Zhang, Y.; Pe-Piper, G.; Piper, D.J.W.; Guo, Z.; Li, W. Permian Rifting Processes in the NW Junggar Basin, China: Implications for the Post-Accretionary Successor Basins. *Gondwana Res.* **2021**, *98*, 107–124. [CrossRef]
66. Jenkyns, H.C. The Early Toarcian (Jurassic) Anoxic Event; Stratigraphic, Sedimentary and Geochemical Evidence. *Am. J. Sci.* **1988**, *288*, 101–151.

67. Psonis, K. *Geological Sheet of Astakos (1:50,000)*; Institute of Geology and Mineral Exploration: Athens, Greece, 1983.
68. Zelilidis, A.; Bourli, N.; Zoumpouli, E.; Maravelis, A.G. Tectonic Inversion and Deformation Differences in the Transition from Ionian Basin to Apulian Platform: The Example from Ionian Islands, Greece. *Geosciences* **2024**, *14*, 203. [CrossRef]